NASA Contractor Report 3058

Experimental Investigation of the Subwing Tip and Its Vortex Structure

James L. Tangler

NASA

NASA Contractor Report 3058

Experimental Investigation of the Subwing Tip and Its Vortex Structure

James L. Tangler
Bell Helicopter Textron
Fort Worth, Texas

NASA

National Aeronautics
and Space Administration

**Scientific and Technical
Information Office**

1978

CONTENTS

LIST OF FIGURES

SUMMARY

Vortex diffusion resulting from the interaction of twin vortices generated by a "subwing" tip was experimentally investigated. The purpose of the investigation was to provide a better understanding of the subwing's vortex structure relative to a square tip for several angle of attack and yaw angles. This comparison included subwings of various chord size and airfoil thickness. Flow visualization, together with performance and wake measurements, provided a comprehensive comparison between the square tip and subwing tips during both a semi-span wind-tunnel test and a small-scale rotor hover-stand test.

Through these studies, the optimum subwing chord to main chord ratio for generating twin vortices was found to be 0.20. By dividing the tip shed circulation into twin vortices, the maximum circumferential velocity in each vortex was lowered relative to a comparable square tip. The influence of yawed flow on the operation of the subwing was not a significant factor for yaw angles corresponding to those that occur on a helicopter rotor blade during partial power descent. Comparisons of subwings having different airfoil thicknesses showed this parameter to be unimportant. No noticeable difference in performance between the subwing and square tip could be detected at medium rotor thrust coefficients.

INTRODUCTION

In forward flight as a helicopter's rotor blade intersects the strong discrete vortices that make up its wake, its per-

formance, structural loads, and acoustic signature are adversely affected. For a two-bladed rotor, these effects are most pronounced during partial power descent. At an advance ratio of 0.15, up to seven discrete intersections can occur over the descent range of 0 to 305 m/sec (1000 ft/sec) as seen in Figure 1 for an AH-1G. Four of these intersections occur in the 1st-quadrant of the rotor disc at blade azimuths of 25°, 42°, 55°, and 70°. In addition, a mid-span intersection occurs across the front of the disc, and two 4th-quadrant intersections occur at azimuths of 280° and 310°. The descent rate where each of these happens is dependent on the twist rate. For negative twist rates greater than 10°, these intersections shift to lower descent rates. The two most important intersections with respect to blade slap noise occur at azimuths of 55° and 70°. These, particularly the former, can induce bow shocks for helicopters having high tip speeds and are the major contributors of the blade slap signature that is heard both in the helicopter cabin and on the ground.

By diffusing the tip vortex prior to its intersection with another blade, the resulting slap signature can be reduced. Several tip shapes (References 1, 2, 3) have been designed for this purpose. One such tip, which is the concern of this investigation, is the "subwing". The advantage of the subwing (Figure 2) relative to other means of vortex diffusion is that it entails only a minor change to the tip region and it appears to produce no significant degradation in rotor performance. The subwing divides the strong concentrated tip vortex into weaker twin vortices. The two vortices then interact to produce turbulence in the opposing flow region between them. The turbulence breaks down the peak core velocities and spreads the vorticity into the surrounding region. The net result of the interaction is one large diffused vortex. The initial design and testing of the subwing is reported on in Reference 1. This study showed that maximum vortex diffus-

2

ion with the subwing is dependent on its location, chord size, span, and incidence. The subwing must be located as far forward and as high on the tip airfoil as possible in order to divide the shed circulation into two vortices of about equal strength and character. Because of these contradictory requirements, the best location is found to be close behind the leading edge and just above the mean chord line. The subwing's chord is the primary parameter used to adjust the relative strength of the two vortices. Although the span also has some effect on the relative strength, its length is chosen such that the twin vortices stay separated and age by themselves as long as possible, but yet combine into one diffused vortex before the following blade passage. This condition produces the highest degree of diffusion in the resultant vortex before it intersects the following blade. During these studies it was also determined that the zero lift line of the subwing should be parallel to the tip airfoil's zero lift line.

The flight test evaluation of the subwing, described in Reference 1, was conducted on a Model OH-58 helicopter. This helicopter was chosen since its tip cap assembly is easily replaced with a tip cap incorporating a subwing. Its low tip speed of 200 m/sec (655 fps) results in mild blade slap relative to helicopter models having much higher tip speeds. Yet the noise measurements obtained in the helicopter cabin during partial power descent indicated that the subwing provided a substantial reduction in the blade slap signature over a square tip. However, following the publication of these results, ground-based noise measurements of the subwing relative to the square tip failed to substantiate the slap reduction detected in the cabin. These contradictory results motivated two simultaneous research efforts at Bell Helicopter Textron (BHT). One of these, an in-house IR&D effort, was directed toward relating the aerodynamic events that occur on the blade during partial power descent to components of the near and far-field slap sig-

nature. The results of this successful research effort are
found in Reference 4. The purpose of the investigation re-
ported herein, was to further study the subwing's vortex dif-
fusion capability, evaluate the subwing's performance, and
determine the influence of yawed flow on the effectiveness of
the subwing. The schlieren method of flow visualization was
used to provide qualitative data on the vortex structure gen-
erated by different subwing geometries relative to a square
tip. In addition, some quantitative data concerning the vortex
structure was also obtained using hot-wire anemometry. The
investigation which was two-part began with a nonrotating semi-
span wind-tunnel test, followed by a small-scale hover-stand
test.

SYMBOLS

AR	aspect ratio
b	blade number
c	subwing chord
C	blade chord
C_D	drag coefficient, $drag/2S\rho V^2$
C_L	lift coefficient, $lift/2S\rho V^2$
C_m	moment coefficient, $moment/2S\rho V^2C$
C_T	rotor thrust coefficient, $thrust/\pi R^2 \rho (\Omega R)^2$
C_Q	rotor torque coefficient, $torque/\pi R^3 \rho (\Omega R)^2$
ℓ	semi-span length measured to pivot bolt
M_T	blade tip Mach number
R	blade radius
S	wing area
V	freestream velocity
V_T	rotor tip speed
V_θ	maximum circumferential velocity in vortex

4

V_τ	translational velocity of vortex
x,y,z	fixed axis system rectangular coordinates
α	geometric angle of attack
β	yaw angle
θ	blade collective pitch angle
ρ	air density
ψ	blade azimuth
ψ_w	azimuth angle measured from a blade to a point on the trailing helical tip vortex filament that originates from the blade
Ω	rotor angular velocity

EXPERIMENTAL APPARATUS

Schlieren System

A schematic of the schlieren system used in both phases of this investigation is shown in Figure 3. It consists of a set of spherical mirrors that provide a field of view 40.6 cm (16 in.) in diameter. They are used in conjunction with a high speed stroboscopic light source that makes a rotating system appear motionless. The light's magnetic pickup, which receives one signal per revolution from the rotor shaft, is coupled to an adjustable time delay circuit. This circuit allows the rotor to be visualized at any azimuth, ψ. The schlieren system can be set to visualize either the vertical or horizontal density gradient of the flow field. Throughout both phases of this investigation, the system was set to visualize the vertical gradient since it best illustrates the structure of a horizontally oriented vortex.

The wind-tunnel schlieren studies, conducted with the semi-span at a tunnel speed of 81.7 m/sec (268 ft/sec), necessitated heating the tip region to enhance the density gradient of the vortex. The hover stand studies conducted at a tip

speed of 152 m/sec (500 ft/sec) provided excellent flow visualization results without the aid of an external heat source.

Semi-Span Model

A full-scale UH-1B tail rotor blade having a 21.3 cm (8.4 in.) chord, 74.3 cm (29.3 in.) span was used for conducting the wind-tunnel studies in the Vought Corporation, 7- by 10-foot, low-speed wind tunnel. The blade had a special tip cap with a removable nose block that could be replaced with the three subwings of different chord size shown in Figure 4. Four 400 watt heat cartridges were housed inside the tip cap to aid the flow visualization of the inboard vortex. The heat from the forward cartridge was vented through four spanwise holes in each subwing to enhance visualization of the outboard vortex. The geometric location of the subwings on the tip is shown in Figure 5.

For the flow visualization studies, the semi-span was installed vertically in the test section on a support system (Figure 6) which permitted the blade pitch angle, yaw angle, and longitudinal position to be varied. Servo motors, which were used to control these parameters, provided ±30° of yaw, 18° of pitch, and 152.4 cm (60 in.) of longitudinal motion. The longitudinal motion of the blade with respect to the schlieren's fixed field of view provided visualization of the wake up to five chord lengths downstream.

A second installation (Figure 7) of the same blade was made onto the tunnel's six-component external balance for measuring performance. In this configuration, the blade's yaw angle was fixed at zero and the pitch angle was varied with the external balance drive system.

Hover Stand Model

The test stand used for the hover studies is shown in Figure 8. It consists of a 30-horsepower, water-cooled motor used to drive a teetering rotor. Thrust measurements are obtained from a small strain-gaged cantilevered beam mounted inside the base of the test stand. A steel ball provides point contact between the end of the cantilever beam and the bottom of the free-sliding steel shaft upon which the drive motor is mounted. The rotor torque reacts against a strain-gaged moment arm mounted to the fixed base just below the drive motor. The absolute accuracy of the thrust and torque measurements is ±2 percent.

The blades, one of which is shown in Figure 9 with the various size sibwings, were milled from laminated pine. The blades had a 61 cm (24 in.) radius, 10.2 cm (4 in.) chord, 10° of twist, and a 0012 airfoil profile. A full-span, brass strip was embedded in the nose of each blade for mass balance and also served as a hard point to which the various size sub-wings could be mounted. The removable upper surface nose block allowed for easy mounting of the subwings. The teetering rotor could be operated in either a one- or two-bladed configuration. As a one-blader, an underslung counterweight was used to create a hub moment equal and opposite to that produced by the sum of the blade's centrifugal force and lift vector.

The tip vortex measurements for the square and subwing tip were taken using a constant-temperature, hot-wire anemometer. A single-sensor, Pt-plated wire probe having a 5 micron diameter and 1.25 mm length was used for this purpose. The signal from the hot-wire was conditioned by a linearizer used to make the output voltage nearly proportional to the flow velocity. The output voltage was monitored on an oscilloscope and select data recorded on magnetic tape at 76.2 cm/sec (30 in./sec).

WIND TUNNEL TESTING

A qualitative comparison of the vortex structure generated by the square tip and three subwings of Figure 4 was conducted with the schlieren. The vortex structure was studied from the trailing edge up to five chord lengths downstream for blade pitch angles of 3°, 6°, 9°, 12° and 15°. Based on this comparison, the subwing found to produce the best matched twin vortices at medium lift coefficients and the square tip were then studied more extensively for yaw angles up to ±30° at blade pitch angles of 6°, 9° and 12°. Performance measurements were obtained for these two tips in the unyawed condition for blade pitch angles from -8° to +20° in increments of 2°. Both the flow visualization studies and performance measurement were conducted at a wind-tunnel speed of 81.7 m/sec (268 ft/sec).

Test Procedure

Flow visualization - The following procedure was used for documenting the tip vortex structure in the wind-tunnel semi-span test. With the semi-span at the desired operating condition, the sensitivity of the schlieren was adjusted for the best contrast. A photograph of the wake was obtained by switching the stroboscopic light source to the single flash mode, exposing the film, and triggering a flash.

Performance measurements - Performance measurements of the subwing that best divides the tip circulation into twin vortices and the square tip were taken with the semi-span mounted to the Vought six-component force and the moment balance. This balance system measures and resolves the forces and moments along and about a set of wind axes having their origin at the center of the test section. The six-component data were then reduced about the semi-span's reference center located at the yaw pivot point as seen in Figure 7. The aerodynamic coefficient data were corrected for model blockage, support tare effects, and static weight tares.

Test Results and Discussion

Flow visualization - The schlieren studies using the semi-span to evaluate the various subwing chord sizes were only marginally successful. Even with the addition of heat, the density gradient in the vortex core was weak, and it was difficult to make a good qualitative comparison between the vortices generated by the three subwings. This was especially true for blade pitch angles less than 12°. The marginal visualization is attributed to the low wind-tunnel speed, 81.7 m/sec (268 ft/sec) and the model's large size. Both of these factors contribute to weaker gradients in the vortex.

Along with the visualization problems resulting from the above factors, the restricted downstream view of the vortices made it difficult to determine qualitatively when the two vortices were of equal strength. Evaluation of their relative strength would have been more easily judged with a much larger field of view of the downstream diffusion process.

Based on a qualitative judgement of the schlieren photographs, the subwing having a chord ratio c/C = 0.226 was chosen as being the best of three subwings to be used for the yawed flow and performance comparisons with the square tip. Shown in Figures 10 and 11 are schlieren photographs of the square tip and chosen subwing at yaw angles of 0, ±10°, ±20°, and ±30° for a blade pitch angle of 9 degrees. The vortex core, which forms close to the airfoil's quarter chord location, always rapidly aligned itself in the direction of the freestream. With the semi-span yawed forward, this trajectory shifts the vortex inboard of the streamwise edge about which it forms; whereas, aft yaw results in the vortex trailing from the quarter chord location, outboard of the streamwise edge. From these photographs it was concluded that for yaw angles up to ±20°, the tip vortex structure of both the square and subwing tip was noticeably affected. However, for forward yaw angles greater than 25 degrees, the vortex structure generated by both the square tip and subwing tip were observed to break down.

With respect to the subwing, the forward yaw reduces the lateral spacing between the twin vortices. This same situation occurs in a rotor's 2nd-quadrant during partial power descent. This is the quadrant in which the rotor generates the segment of the vortex system that it later intersects while rotating through the 1st-quadrant. However, the reduced lateral spacing between the vortex pair that results from forward yaw is partially offset by increased vertical spacing that results from an increase in angle of attack as the blade rotates through the 2nd-quadrant. Because of these compensating effects and the fact that the yaw angle doesn't exceed 8.5° (advance ratio = 0.15) during partial power descent, the effect of yaw on the interaction of the twin vortices is not a significant factor. This is further verified by related small-scale partial power descent studies using a two-bladed nontwisted rotor at an advance ratio of 0.15 as shown in Figure 12. During this test it was observed that the relative strength of the two vortices and the resulting interaction was not affected by the yawed flow but does show some variation with disc loading. At low disc loadings, the subwing's vortex is slightly stronger than the inboard vortex; whereas at high disc loading, the reverse is true. Consequently, it is necessary to size the subwing for a specific blade loading range.

Performance measurements - A comparison of the force data for the chosen subwing and square tip is shown in Figure 13. In the C_L versus α plot it is seen that the lift curve slope with the subwing installed is 4.4 percent greater than that of a square tip. Based on the difference in aspect ratio, an increase of this magnitude is reasonable. A comparison of the drag coefficient for the two tips shows little difference up to a pitch angle of 14°. Beyond that point, the drag coefficient of the subwing becomes larger. A comparison of the moment coefficient shows that the subwing produces a more nose-up moment due to its placement at the semi-span's leading edge.

10

HOVER STAND TESTING

The flow visualization studies of the small-scale sub-wings, shown in Figure 9, were conducted on the model rotor hover test stand using a one-bladed rotor. The studies were conducted for the purpose of determining the best subwing chord size at medium thrust coefficients. This corresponds to three-quarter radius collective pitch angles of 6°, 9° and 12°. Two of the four subwings were scaled-down versions of the semi-span subwings that had subwing-chord to main-chord ratios of 0.20 and 0.23 and a NACA 0012 airfoil section. In addition, two thicker subwings having a NACA 0016 airfoil section and subwing-chord to main-chord ratios of 0.20 and 0.18 were also evaluated to determine if there was a tradeoff between subwing chord size and airfoil thickness.

Along with the flow visualization studies, some quantita-tive information concerning the vortex structure of the square tip and the subwing having the best diffusivity was obtained using a hot-wire anemometer. Velocity measurements were ob-tained at various points along the vortex trajectory at a col-lective pitch of 9°. The vortex studies were conducted using a one-bladed rotor since its inflow distribution in the tip region better approximates the inflow across the front of the disc during partial power descent than does a two-bladed hover-ing rotor. For a two-bladed hovering rotor, the presence of the preceding blade's tip vortex below the blade produces sub-stantial upwash on the subwing which puts it at an angle of at-tack relative to the blade not representative of partial power descent. As previously mentioned, that segment of the vortex that intersects the blade in the 1st-quadrant during partial descent is generated across the front of the disc outside the influence of previous vortices.

Performance of the chosen subwing and square tip was com-pared in both a one- and two-bladed configuration. Tipspeeds

11

of 152 m/sec (500 ft/sec) and 183 m/sec (600 ft/sec) were run for the one-blader; whereas, only 152 m/sec was run for the two-blader due to the limitation of the test stand's thrust member.

Test Procedure

Tip vortex measurements - A stationary hot-wire probe was positioned along the vortex trajectory to record the velocity distribution through the vortex. Figure 14 shows the probe's orientation with respect to the blade. The hot-wire lies in a horizontal plane and is perpendicular to a radial originating at the rotor's center of rotation. The wire is sensitive to that component of velocity normal to its axis and relatively insensitive to that component of velocity along its axis which is assumed to be small. Prior to taking velocity measurements the hot-wire was calibrated against a cistern type manometer from zero to 110 m/sec (360 ft/sec). The probe was then positioned at the desired axial location below the disc. With the rotor at operation rpm, the relationship of the hot-wire to the tip vortex trajectory was observed on the viewing screen of the schlieren system. The probe was then traversed radially to intersect the trajectory. As the tip vortex passed over the hot-wire each revolution, the velocity distribution was monitored on an oscilloscope and recorded on magnetic tape.

Performance measurements - The following procedure was used to measure the performance at each collective pitch setting. First the blade's collective pitch was set using a clinometer. This was always done with the blade positioned to the same azimuth. Prior to taking data at each collective pitch angle, the rotor was run up to operating rpm and back to rest in order to eliminate any static preset in the force-measuring elements of the test stand. The outputs for thrust and torque were then zeroed with the rotor at rest. The rotor was then run up to the desired test rpm. After the inflow through the disc stabilized,

12

thrust and torque data were recorded. The rotor was then brought back to rest, and the thrust and torque outputs were checked for zero shifts. Calibration readings were recorded after each test point. The thrust load cell was calibrated by setting weights on the rotor hub while the torque cell was calibrated by applying a known force to a known moment arm. Ambient temperature and pressure were recorded during the test.

Test Results and Discussion

Flow visualization - Results from the one-bladed flow visualization studies are shown in Figures 15 through 23 for collective pitch angles of 6° and 9°. These composite photographs illustrate the diffusive interaction of twin vortices versus a single vortex up to 1-1/2 revolutions below the rotor. Comparisons at 12° were impractical since the tip region for all four subwings was partially stalled at this collective.

Figures 15 and 16 show the structure of the vortex generated by the baseline square tip rotor for the two collective pitch angles. The vorticity in the tip region is seen to form into a concentrated core within one chord length behind the trailing edge. The core diameter (0.03C at $\theta=6°$ and .06C at $\theta=9°$) remains relatively constant with distance downstream and little vortex diffusion occurs over the region shown. In Reference 5, it was found that the core structure remains intact up to four revolutions downstream for a one-bladed rotor.

Through the use of the subwing, the vortex diffusion process is accelerated. The turbulence produced by the intersection of twin vortices transports their vorticity into the surrounding area. By the time the vortices are one-rotor-revolution old, evidence of their discrete core structure becomes difficult to detect. Figures 17 and 18 show the twin vortices generated with the large chord subwing (c=0.23C) for both collective pitch angles. To aid in tracking the two vortices, the

subwing vortex is designated by the letter "A" and the inboard vortex is designated by the letter "B". Here it is seen that the subwing vortex "A" is slightly greater in strength than the inboard vortex "B". Because of this difference, the stronger subwing vortex is seen to persist further downstream than does the inboard vortex.

Figures 19 and 20 show the vortices generated with the medium chord subwing (c/C=0.20) at the same conditions. For this case, the twin vortices are seen to be closely matched in strength at all azimuths which is a prerequisite for maximum diffusion (Reference 1). It is also seen that the diffusion process occurs slightly faster for the higher collective pitch setting. This optimum chord size for the model is slightly smaller than that indicated by the semi-span results; however, it is in agreement with the full-scale subwing flight test results from the Model OH-58 (Reference 1). By comparing Figure 21 to Figure 19, the changes in the wake structure resulting from increasing the airfoil thickness from 12 percent to 16 percent for the medium chord subwing (c/C=0.20) can be observed. In both cases, the twin vortices are closely matched in strength which indicates airfoil thickness is of minor importance.

Figures 22 and 23 show the vortices generated by the small chord (c/C=0.18), 16 percent thick, subwing. The inboard vortex "B" is seen to be slightly stronger than that produced by the subwing. This difference is most noticeable after the vortices are one-half revolution old as seen for blade azimuths of 180°, 240° and 330°.

Based on the qualitative flow visualization evaluation, the parametric sweep of the subwing's chord size indicates for the medium thrust coefficient range, a subwing chord to main chord ratio of 0.20 is nearly optimum. This size has been found to divide the tip vorticity into two vortices of approximately equal strength and character. Changes in the relative strength

14

of the two vortices were not noticeably affected by an increase
in airfoil thickness.

Tip vortex measurements - Several factors complicated the
task of obtaining useful data with the hot-wire anemometer.
For a one-bladed rotor, the tip vortex meanders extensively
about its mean path compared to a multi-bladed rotor. Because
of this, longer data sampling times are required, especially
downstream where the excursions become larger. In the case of
the subwing, this meandering was also compounded as the twin
vortices revolved about their common centroid of vorticity.
Also, since the subwing vortex stays close to the plane of ro-
tation because of the inboard vortex's induced effect, it can-
not be probed with the hot-wire until it is almost one-half of
a revolution old.

Interpretation of the hot-wire traces that were obtained
with the stationary probe is based on several assumptions.

1. The hot-wire is assumed to be parallel to the vortex
    being measured; that is, the curvature of the vortex is
    small along the length of the wire.

2. The cooling produced by the axial component of the core
    velocity is assumed to be small since the wire is rela-
    tively insensitive to this component of the flow.

3. The stagnation temperature change in the vortex is assumed
    to be small.

4. The translational velocity of the vortex across the sta-
    tionary probe is assumed to be constant during the time
    required for the vortex to cross the hot-wire.

5. The vortex is assumed to be symmetrical over the interval
    investigated.

As the vortex intersects the hot-wire located along its
trajectory, the vector sum of the maximum circumferential ve-
lcoity in the vortex and the translational velocity of the vor-
tex are measured by the wire as seen in Figure 24. The signal
differs considerably depending on what portion of the vortex

passes over the wire. If the inside portion of the core inter-
sects the wire (Point A), the wire measures the quantity $V_\theta + V_\tau$;
whereas, if the outside edge of the core intersects the wire
(Point B), the quantity $V_\theta - V_\tau$ is measured. The case of primary
concern is when the center of the core intersects the wire
(Points C and D). When this occurs, the quantity $\sqrt{V_o^2 + V_\tau^2}$
is measured as the top and bottom edge of the core intersect
the wire.

The velocity distribution measured by the hot-wire about
eight chord lengths ($\psi = 75°$) downstream of the square tip for
$\theta = 9°$ is shown in Figure 25. The trace, which is representative
of those measured up to one revolution downstream, moves from
left to right. The hot-wire first senses the induced velocity
from the blade bound vortex as it passes over the probe. Then,
as the tip vortex intersects the wire, two peaks appear which
correspond to the edge of the core and points C and D of Figure
24. Inside the vortex core, the circumferential velocity in-
creases from zero at the center to a maximum at the core's
boundary. Outside the core, the circumferential velocity drops
off at a rate inversely proportional to the distance from the
center. The maximum circumferential velocity was obtained by
subtracting the translational velocity of the vortex across the
wire from the peak velocity at the edge of the core. The trans-
lational velocity was determined from a series of schlieren
photographs that depict its motion versus time.

Examination of the hot-wire trace shows assumption No. 5,
concerning the symmetry of the vortex, to be questionable. In
all cases where there appeared to be an intersection of the
center of the vortex core the velocity trace indicated the up-
per half of the vortex just outside the core to be wider and
to have a larger peak magnitude. The upper half's velocity
distribution is also choppy compared to the lower half. These
observations are unexpected since similar rotor investigations
did not encounter significant vortex asymmetry (References 6

16

and 7). The most likely cause of the asymmetry appears to be a disturbance to the vortex by the probe. Any disturbance created by the probe as it enters the lower half of the vortex would be carried around to the upper half before that portion of the vortex intersects the hot-wire. Consequently, it appears that only the lower half of the velocity distribution should be used for analyzing the characteristics of the vortex.

From the velocity distribution of Figure 25, the core diameter is measured to be 6 percent of the tip chord at this collective pitch. By subtracting the translational velocity of the vortex core (6.7 m/sec or 185 ft/sec), the maximum circumferential velocity for this case is found to be 33 percent of the tip speed.

Figure 26 shows the velocity distribution through the two nearly equal vortices generated using the chosen subwing (c/C=0.20) configuration at a collective pitch of 9 degrees. The measurement for the inboard vortex was obtained about eight chord lengths downstream; whereas for the subwing's vortex, the measurement corresponds to fifteen large chord lengths downstream. The core diameter for the subwing vortex is slightly smaller than the standard square tip; whereas, the inboard vortex has about the same core size as the vortex generated by the square tip. The maximum circumferential velocities of the twin vortices prior to the diffusive interaction is at least 20 percent less than the standard square tip. Again, due to the vortex asymmetry, only the velocity distribution corresponding to the lower half is considered to be accurate. Although there is a substantial reduction in the maximum circumferential velocities of the two vortices this does not imply a reduction in shed vorticity relative to the comparable square tip.

Performance measurements – The performance comparison between the subwing and square tip in a one- and two-bladed rotor configuration is shown in Figure 27. In calculating the thrust and torque coefficients the 61 cm (24 in.) radius of the square

tip blade was also used as the reference radius for the blade with the subwing tip. Consequently, the tipspeeds indicated in Figure 27 correspond to this radial station. For each rotor, data were obtained up to the thrust limit of the test stand. The performance trends shown are in general agreement with the semi-span force measurements. At $C_T=0$, it is seen that the subwing requires slightly more profile power because of the resulting radius increase. At medium thrust coefficients, the increase in radius or aspect ratio provides a performance improvement of about 2 percent more thrust at a given power. At high thrust coefficients, the subwing results in a slight performance loss. The schlieren shows that this results from premature leading edge separation over the inboard portion of the subwing (Figure 28). The separation appears to be due to the upwash induced on the subwing by the inboard vortex. The resulting increase in the angle of attack on the inner portion of the subwing then leads to early separation and stall relative to the main blade. The tubrulence resulting from the separation is seen to be entrained by the inboard vortex rather than the subwing's vortex.

<div align="center">CONCLUDING REMARKS</div>

Through these studies, the optimum size subwing for generating twin vortices of equal strength at medium thrust coefficients was found to have a subwing-chord to main-chord ratio of 0.20. By dividing the tip circulation into twin vortices with the subwing, the maximum circumferential velocity in each vortex was measured to be lower than for a comparable square tip. The influence of yawed flow on the operation of the subwing was not a significant factor for yaw angles corresponding to those that occur during partial power descent. A comparison between subwings having different airfoil thicknesses for a constant chord size showed this parameter to be unimportant.

The performance comparison between the subwing and square tip showed that the increased radius due to the subwing slightly increased the profile power. Evidence of this is seen for a thrust coefficient of zero. However, at medium thrust coefficients, this radius increase provides a slight performance improvement which is predictable based on the difference in aspect ratio. At high thrust coefficients, early flow separation occurs on the subwing due to the upwash from the inboard vortex. The requirement to locate the subwing near the leading edge results in an increase in the nose-up moment coefficient.

Although the results of this investigation indicate the subwing can rapidly diffuse the tip vortex without significantly altering the rotor's performance, further study is necessary to determine if the resulting reduction in partial-power-descent blade-slap signature justifies its use. The results of Reference 4 suggest that vortex diffusion type tips are most beneficial for rotors having tip speeds in excess of Mach 0.7 where compressibility effects due to blade/vortex interaction begin to dominate the partial power descent slap signature. This observation helps explain the discrepancy between the OH-58's cabin and ground based blade-slap noise measurements mentioned in the introduction. Although the use of the subwing on this helicopter provided a noticeable reduction in the slap signature component heard in the cabin during partial power descent it appeared to have no effect on the noise signature measured on the ground because of the OH-58's low tip speed of Mach 0.586. Most likely the mild signature heard on the ground is dominated by the blade thickness component. This component of the signature has a forward directivity in the rotor plane and cannot be heard in the helicopter's cabin (References 4, 8). Whereas, that component of the signature due to blade/vortex interaction that originates behind the cabin and has a forward directivity along an azimuth 30 degrees below the rotor plane propagates across the cabin and is heard inside. However, to a

ground-based observer, this component of the signature is weak compared to the blade thickness component for low tip speed rotors. Only for high tip speeds helicopters such as a UH-lH, does the blade/vortex component of the slap signature dominate what a ground based observer hears during partial power descent.

REFERENCES

1. Tangler, J. L.: The Design and Testing of a Tip to Reduce
    Blade Slap. AHS Paper 963, presented at the 31st Annual
    National Forum of the American Helicopter Society, May
    1975.

2. Mantay, W. R.: Some Results of the Testing of a Full-Scale
    Ogee Tip Helicopter Rotor; Acoustics, Loads and Perform-
    ance. AIAA Paper 77-1340, Presented at the AIAA 4th
    Aeroacoustics Conference, October 1977.

3. White, R. P. and Balcerak, J. C.: An Investigation of the
    Mixing of Linear and Swirling Flows. RASA Report 72-04,
    February 1972.

4. Tangler, J. L.: Schlieren and Noise Studies of Rotors
    in Forward Flight. AHS Paper 77, 33-05, Presented at the
    33rd Annual National Forum of the American Helicopter
    Society, May 1977.

5. Kocurek, J. D., and Tangler, J. L: A Prescribed Wake
    Lifting Surface Hover Performance Analysis. AHS Paper
    1001, Presented at the 32nd Annual National Forum of the
    American Helicopter Society, May 1976.

6. Cook, C. V.: The Structure of the Rotor Blade Tip Vortex.
    Presented at AGARD Specialists' Meeting on Aerodynamics
    of Rotary Wings, (Marseille, France), September 1972.

7. Tangler, J. L., Wohlfeld, R. M., and Miley, S. J.: An
    Experimental Investigation of Vortex Stability, Tip
    Shapes, Compressibility, and Noise for Hovering Model
    Rotors. NASA CR-2305, September 1973.

8. Schmitz, F. H., and Boxwell, D.A.: In-Flight Far Field
    Measurement of Helicopter Impulsive Noise. Journal of
    the American Helicopter Society, Vol. 21, No. 4, October
    1976.
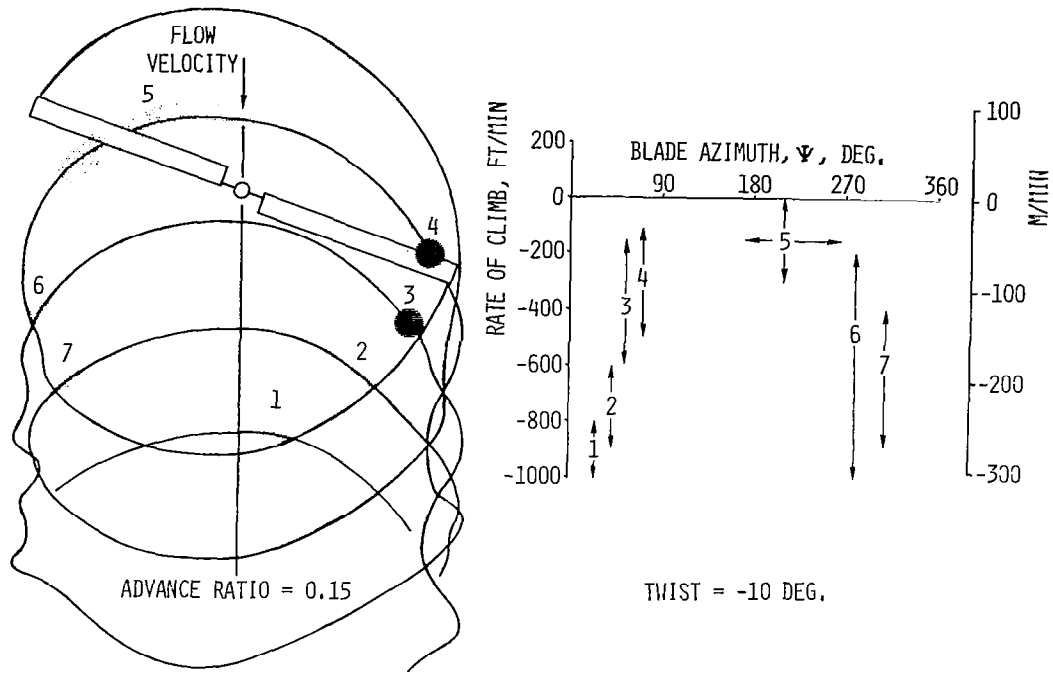
Figure 1. Blade/vortex intersections during partial power descent.
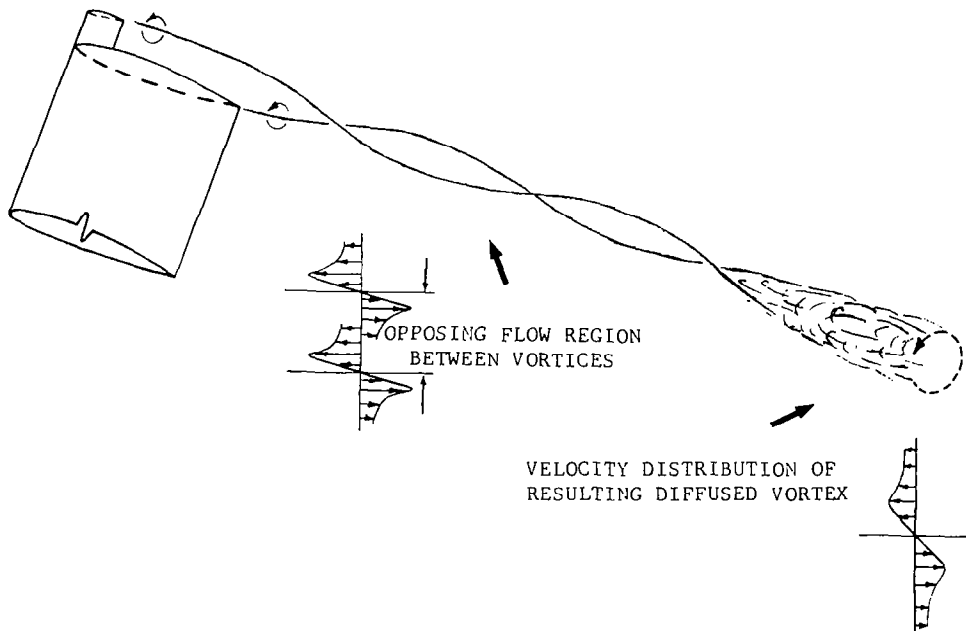
Figure 2. Twin vortices generated by the subwing tip.
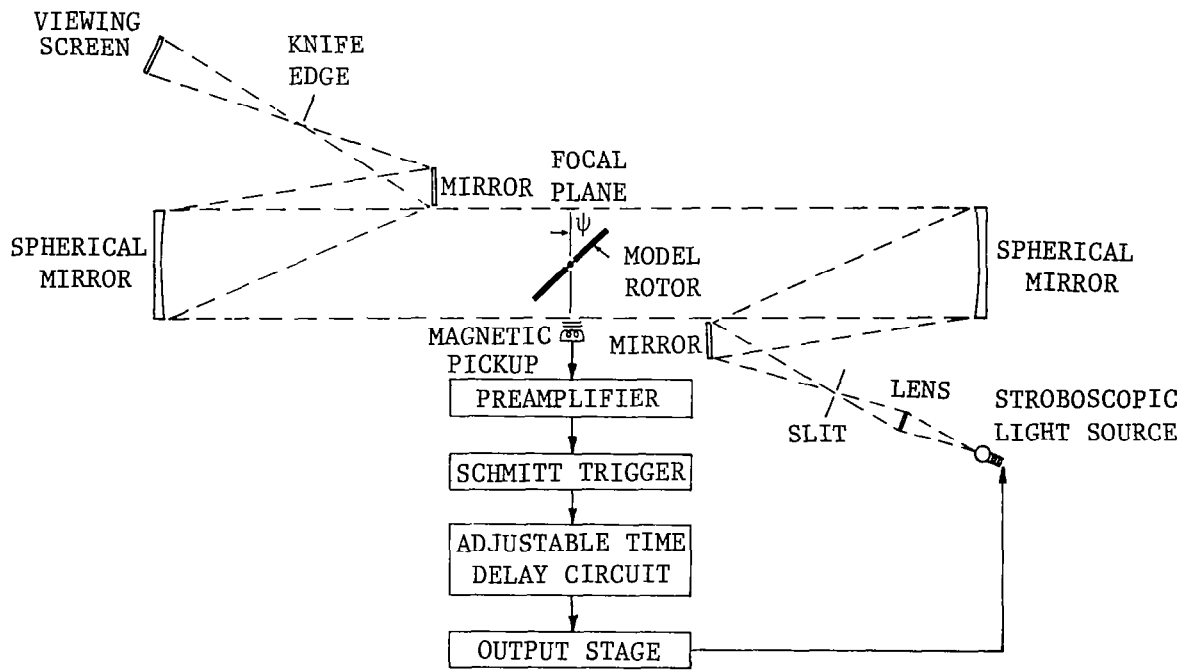
Figure 3. Schematic of the schlieren system.
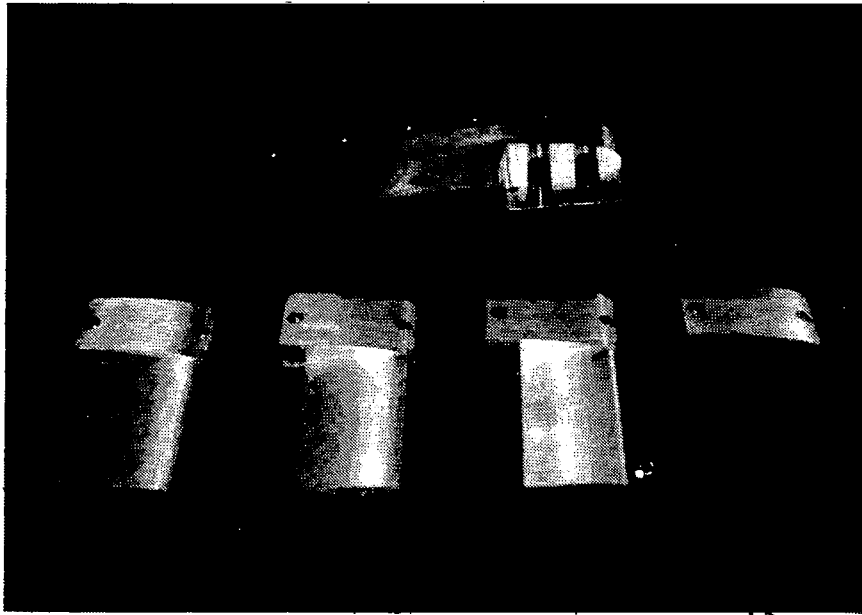
c/C = 0.250   c/C = 0.226   c/C = 0.202

Figure 4.   Semi-span tip cap with removable subwings.
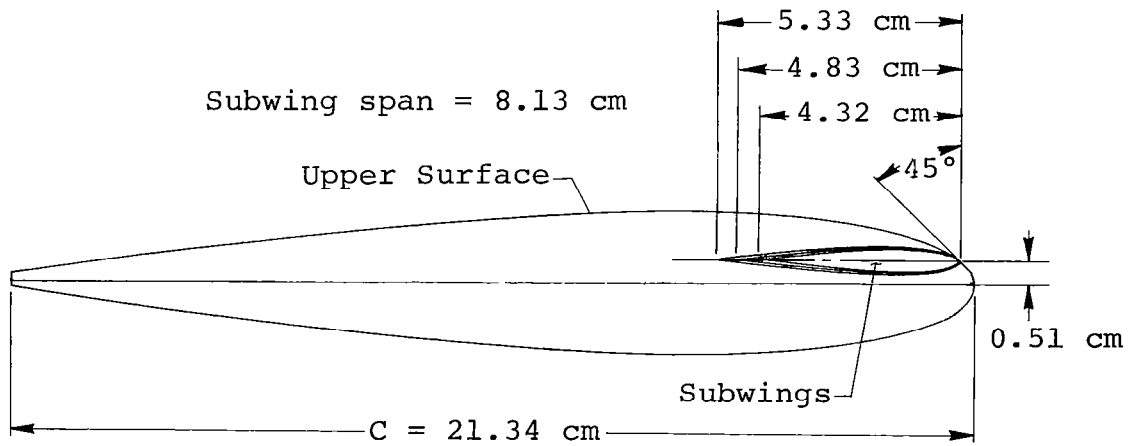
Figure 5.   Schematic showing location and size of the subwings.

c = 0.213m (0.700 ft)
ℓ = 0.743m (2.438 ft)
S = 0.158 m^2(1.706 ft^2)
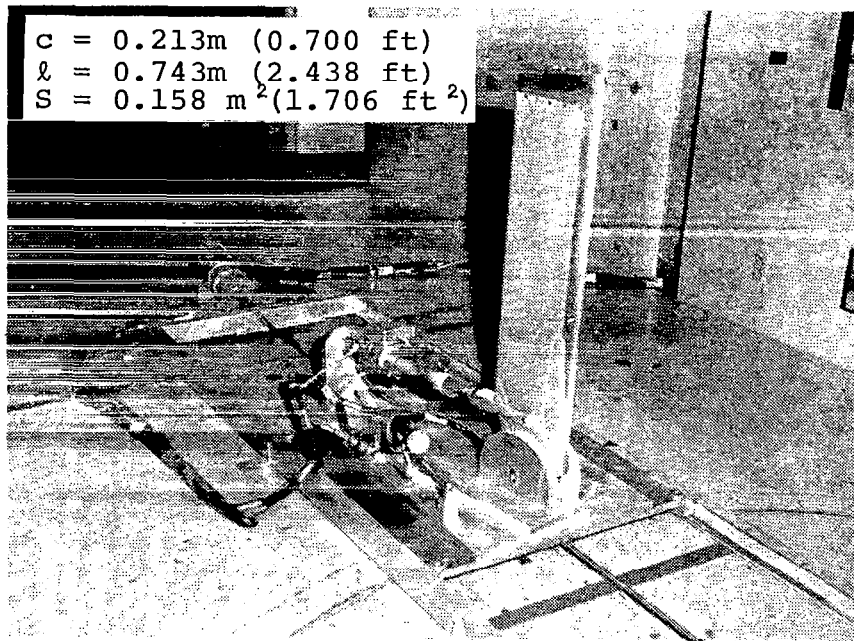
Figure 6.   Installation of semi-span for flow visualization
            studies.

Yaw pivot
point
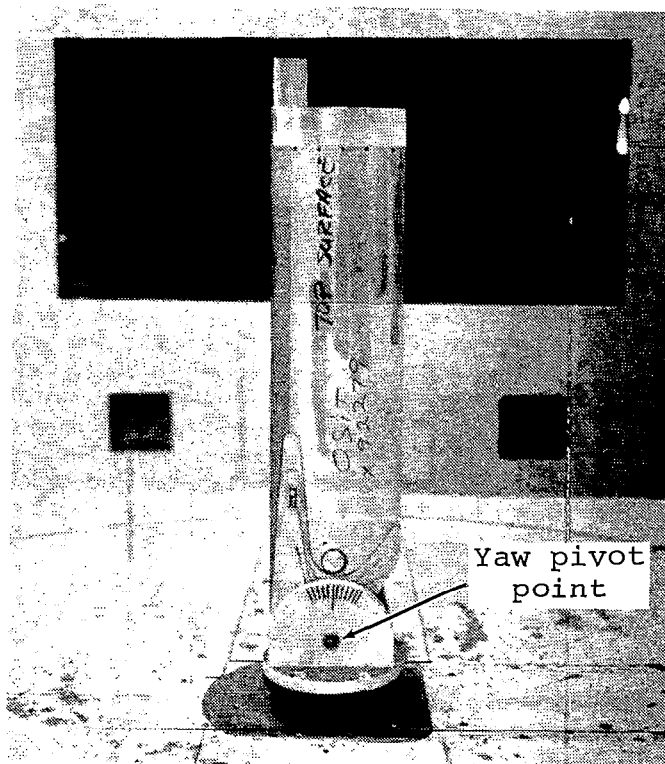
Figure 7.   Installation of semi-span on external balance for
            force and moment test.
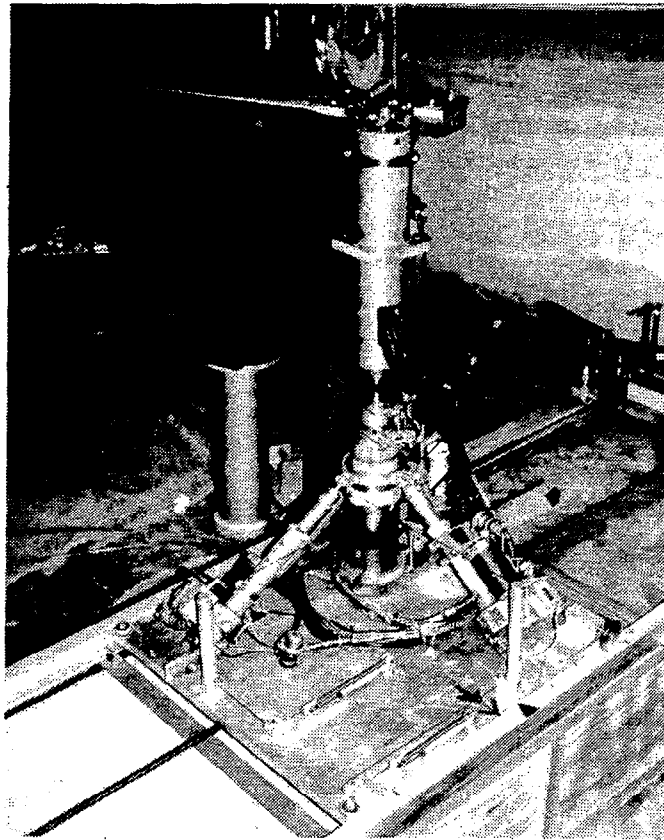
Figure 8.   Model rotor hover test stand.
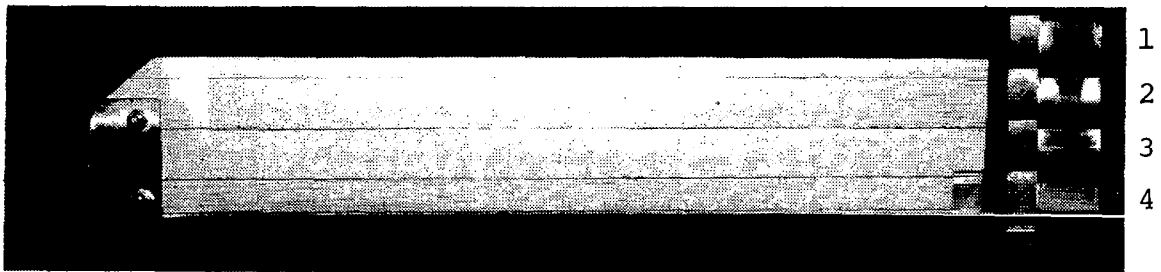
Subwing No.	Chord Ratio	Airfoil Section
1	0.23	NACA 0012
2	0.20	NACA 0012
3	0.20	NACA 0016
4	0.18	NACA 0016

Figure 9.   Model blade with removable subwings.

26

β=-30°

β=30°

β=-20°

β=20°

β=-10°

β=10°

Freestream, V

Angle of attack, α=9°
V=81.7 m/sec (268 ft/sec)

L.E.

β=0°
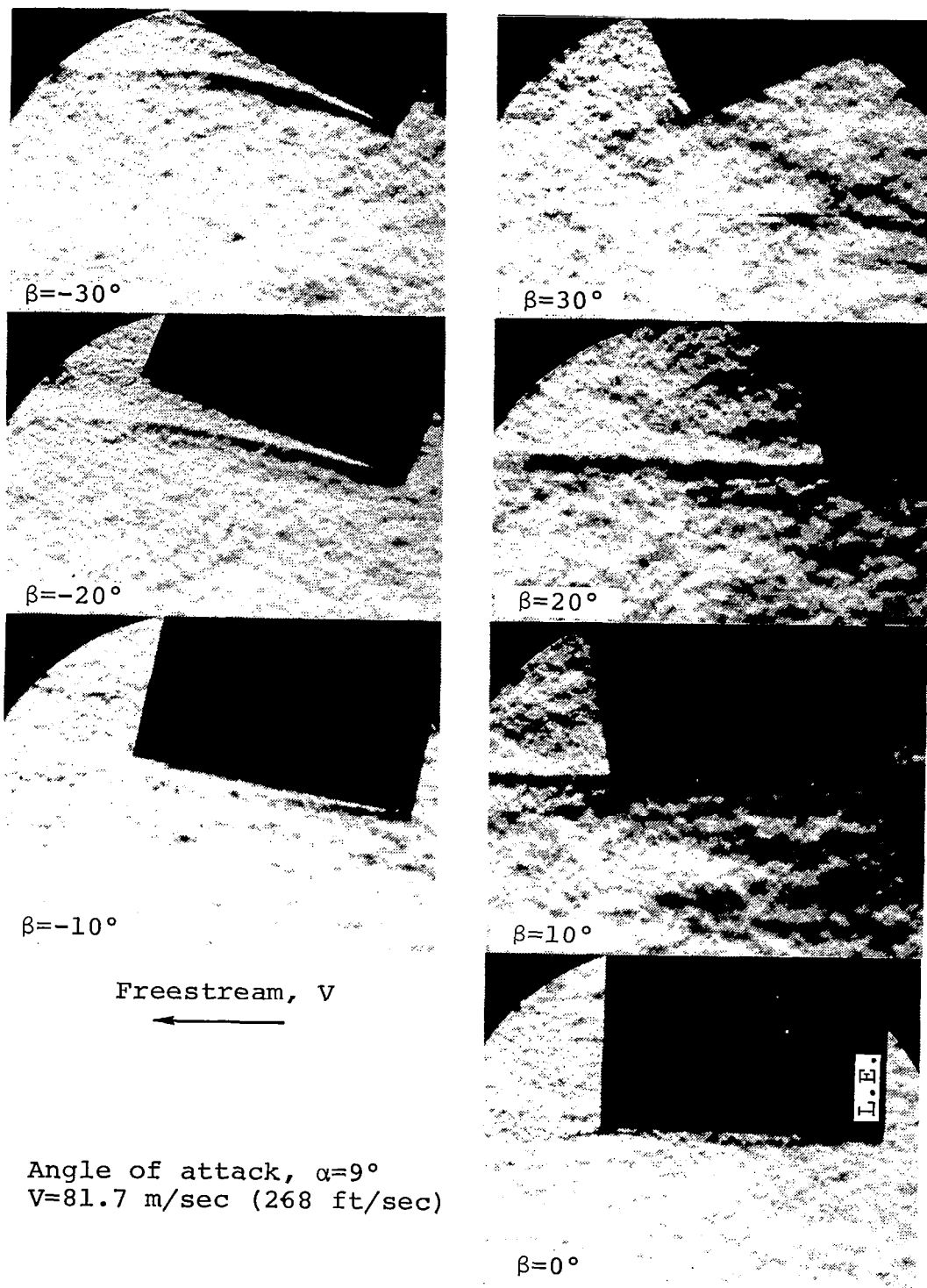
Figure 10. Tip vortex generated by the square tip semi-span
at several yaw angles.

β=-30°

β=30°

β=-20°

β=20°

β=-10°

β=10°

Freestream, V

Angle of attack, α=9°
V=81.7 m/sec (268 ft/sec)

L.E.

β=0°
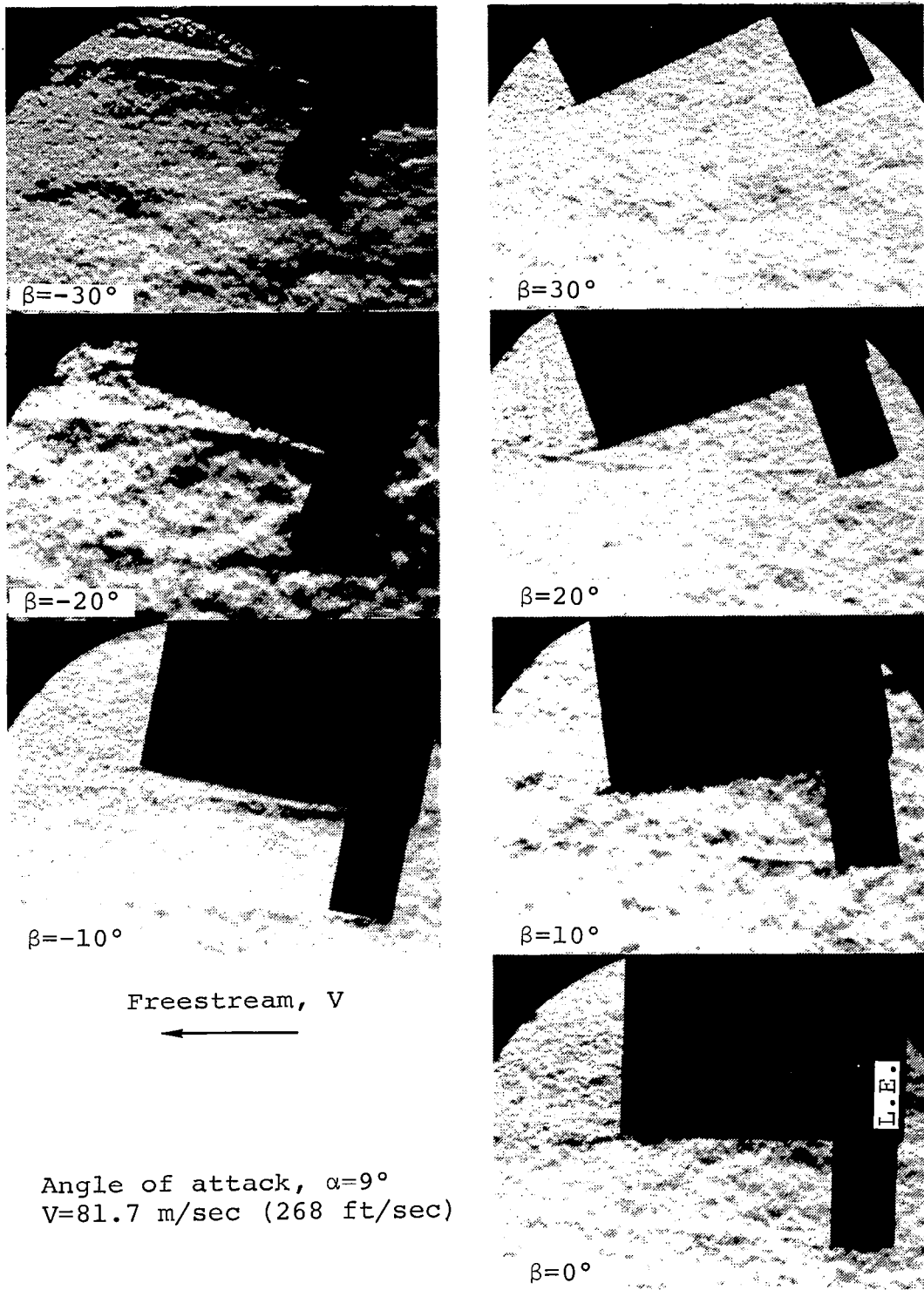
Figure 11.   Tip vortex generated by the subwing tip semi-span
             at several yaw angles.

28
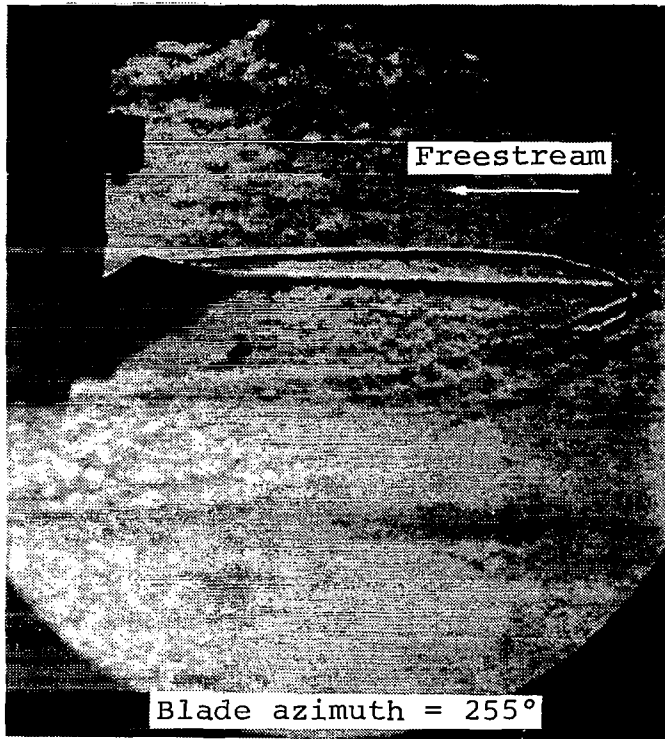
Tip speed = 228.6 m/sec (750 ft/sec)
Advance ratio = 0.15
Descent rate = 121.9 m/sec (400 ft/sec)
Disc loading = 36.6 kg/m^2 (7.5 lb/ft^2)

Figure 12. Vortex structure generated by a small-scale
subwing during simulated partial power descent.
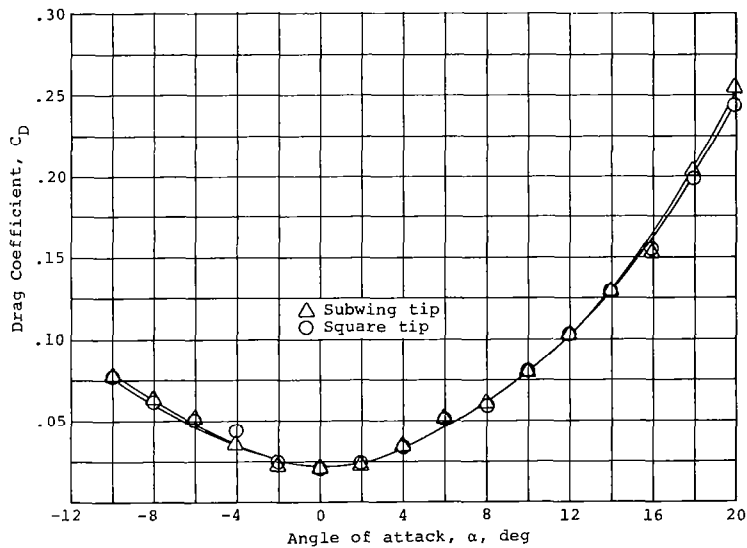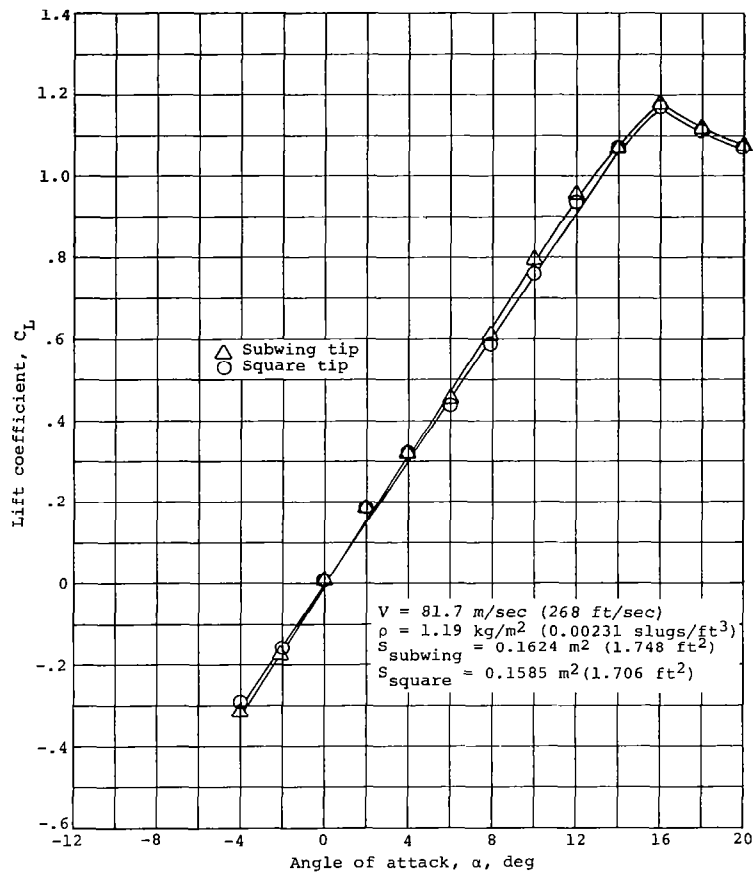
Figure 13. Force and moment data for the semi-span model.
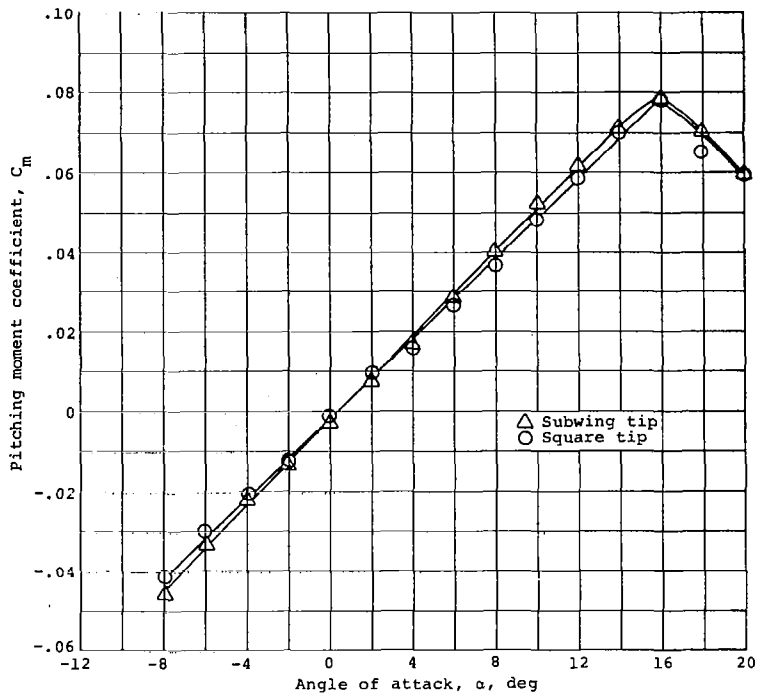
Figure 13.   Concluded.
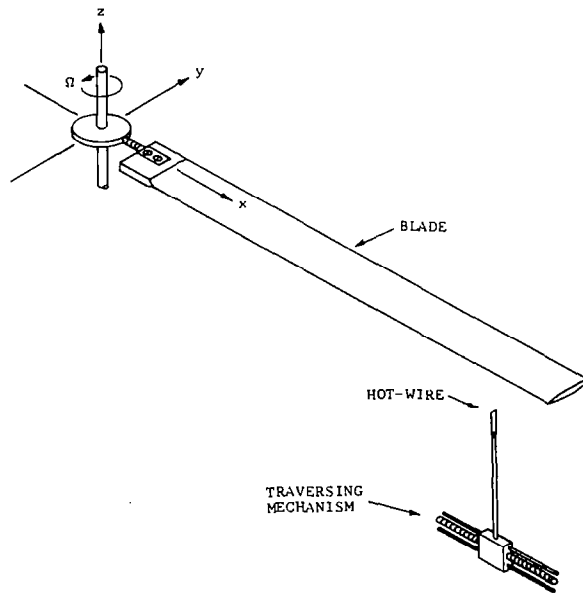
Figure 14.   Stationary hot-wire anemometer relative to
the blade.

31
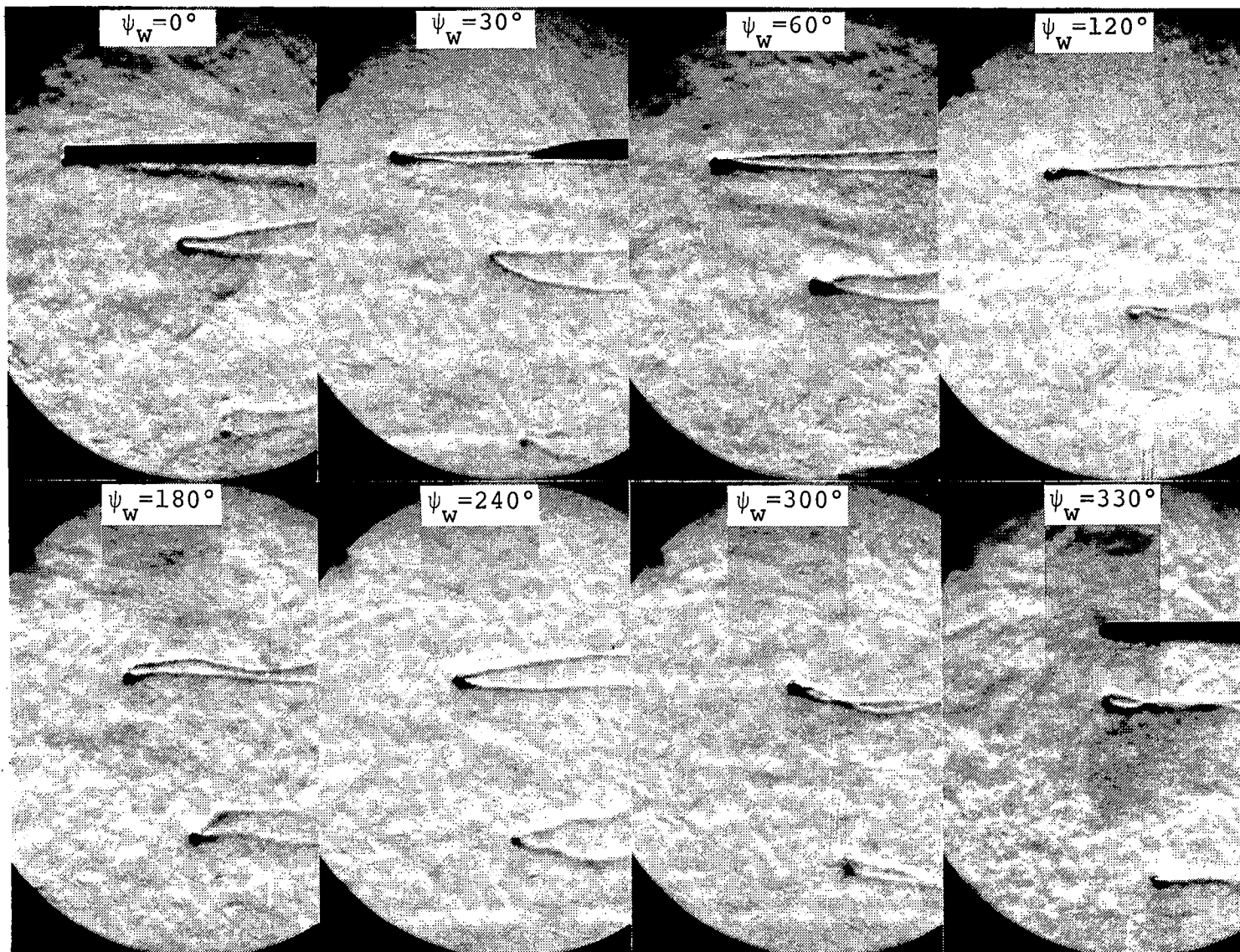
Figure 15.   Wake generated by the square tip rotor at θ=6°, b=1, V_T=152 m/sec.
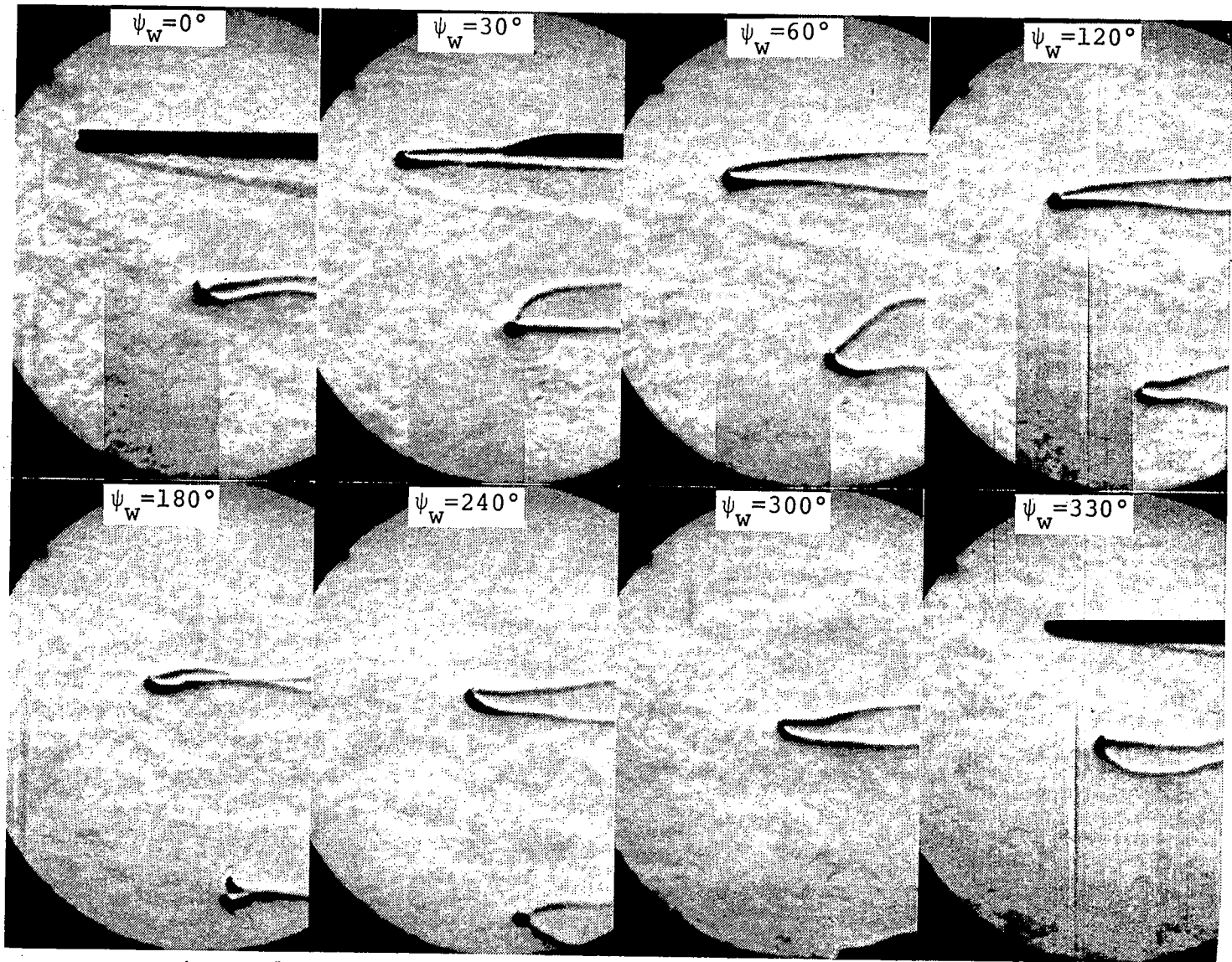
Figure 16. Wake generated by the square tip rotor at $\theta=9°$, $b=1$, $V_T=152$ m/sec.
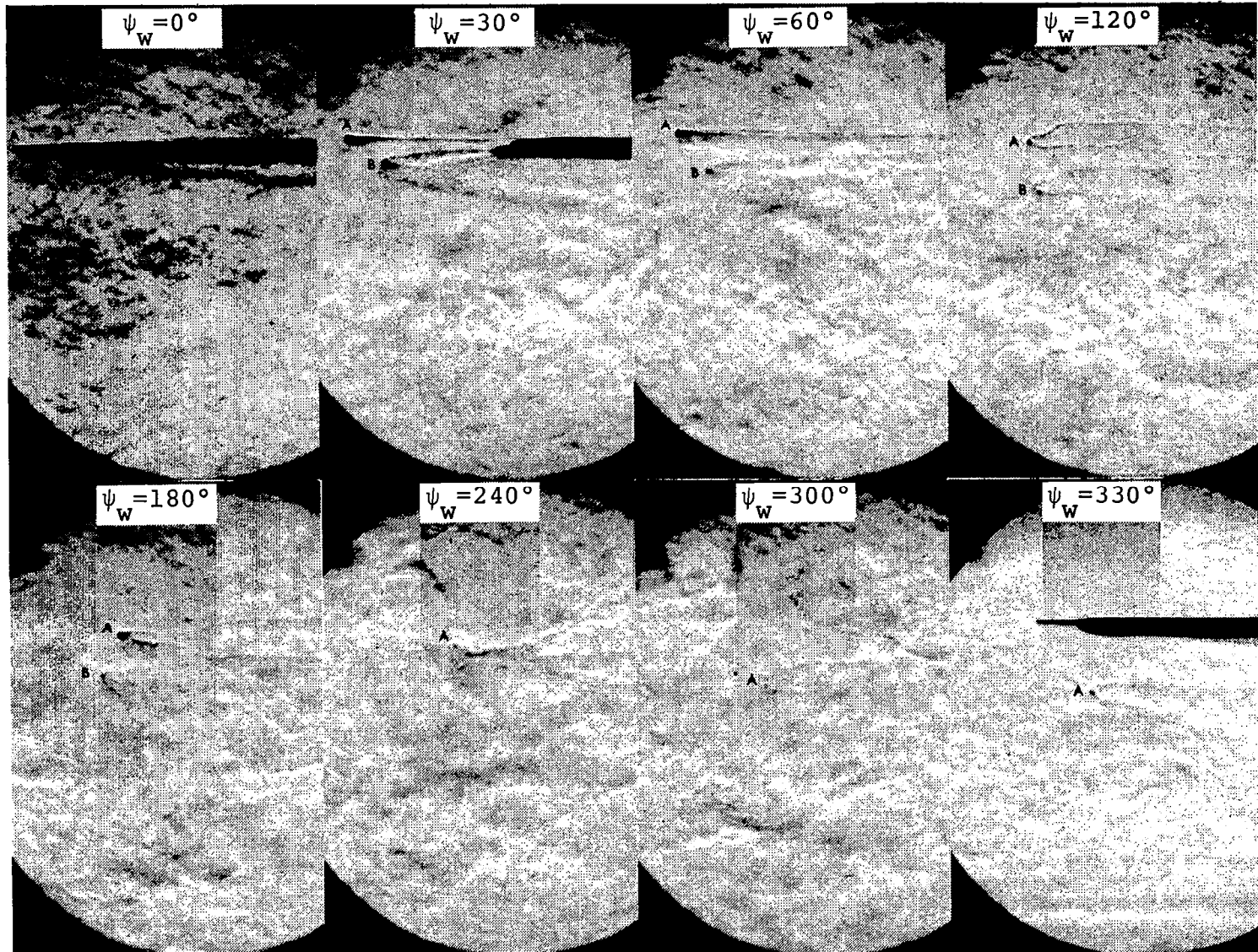
Figure 17.   Wake generated by the subwing tip (c=0.23C, NACA 0012 airfoil)
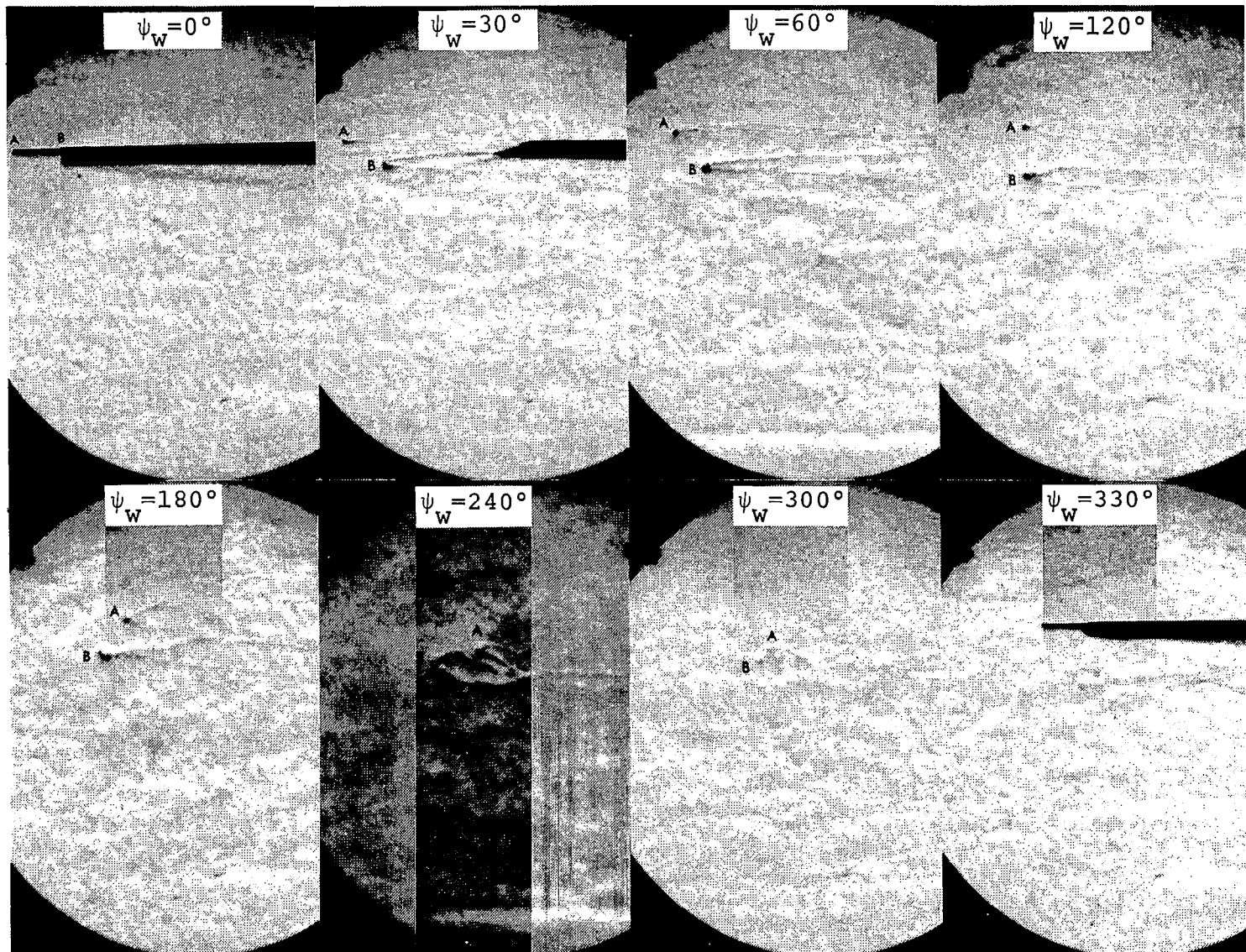rotor at $\theta=6°$, b=1, $V_T=152$ m/sec.
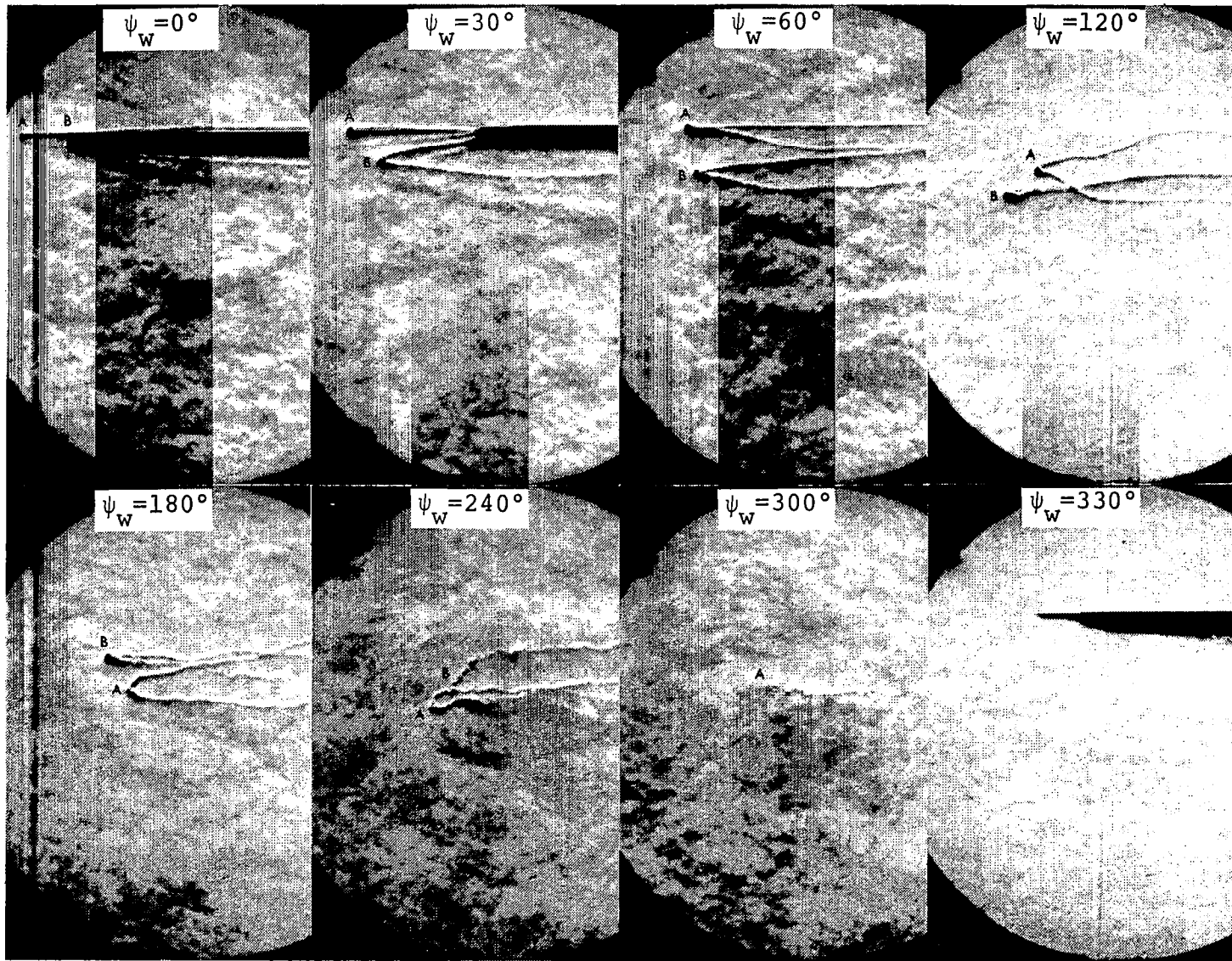
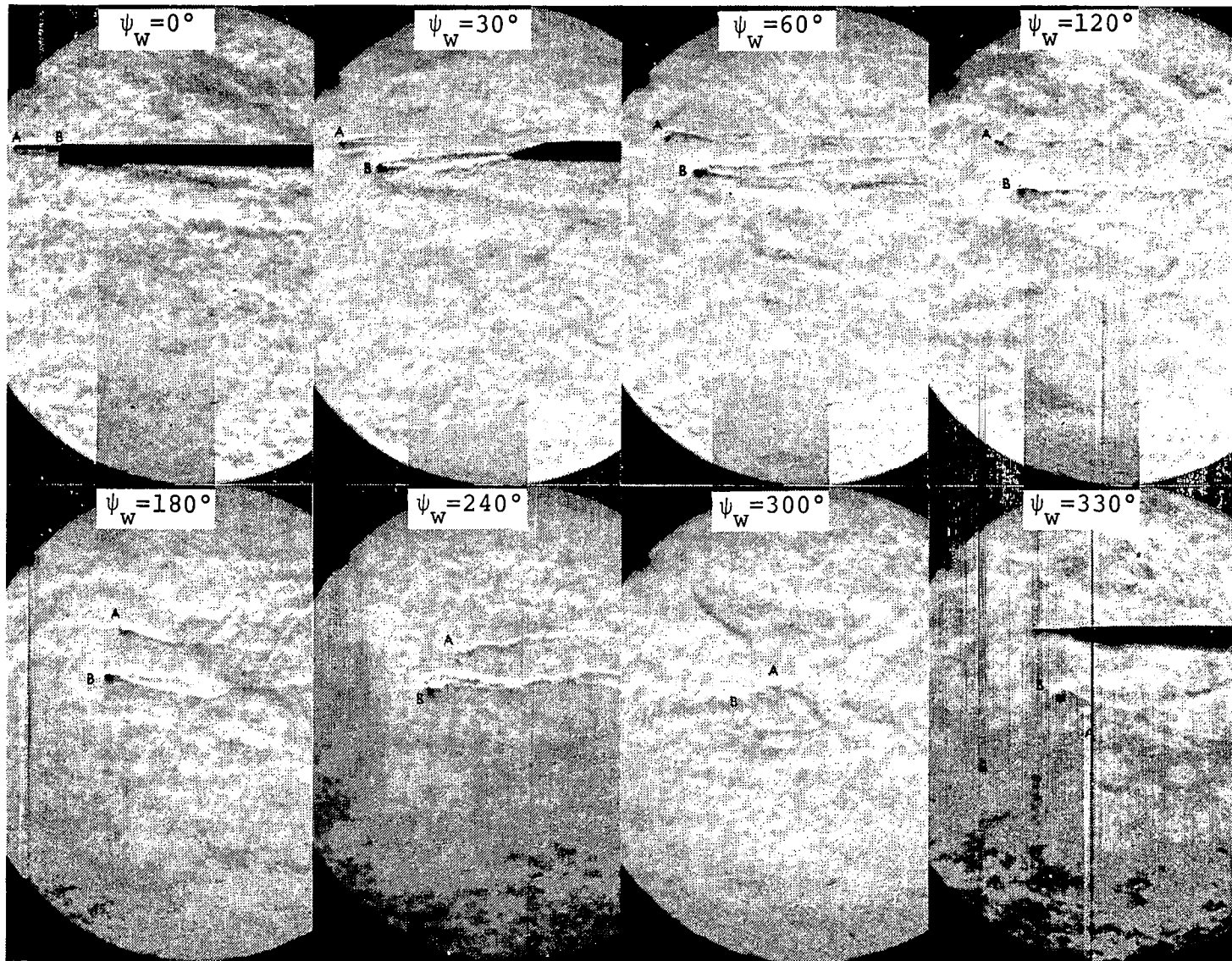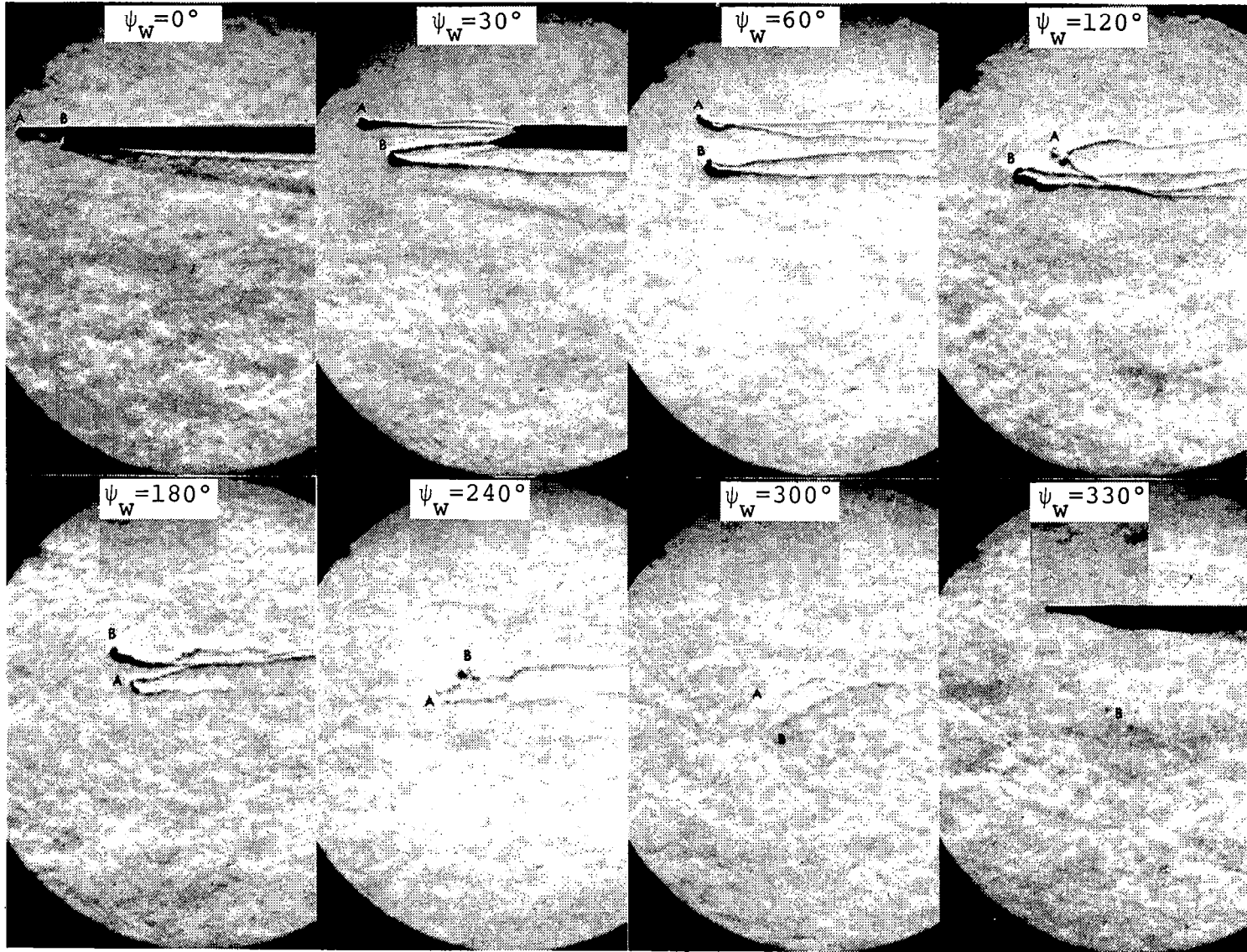Figure 18. Wake generated by the subwing tip (c=0.23C, NACA 0012 airfoil) rotor at θ=9°, b=1, V_T=152 m/sec.

Figure 19.   Wake generated by the subwing tip (c=0.20C, NACA 0012 airfoil)
             rotor at θ=6°, b=1, V_T=152 m/sec.
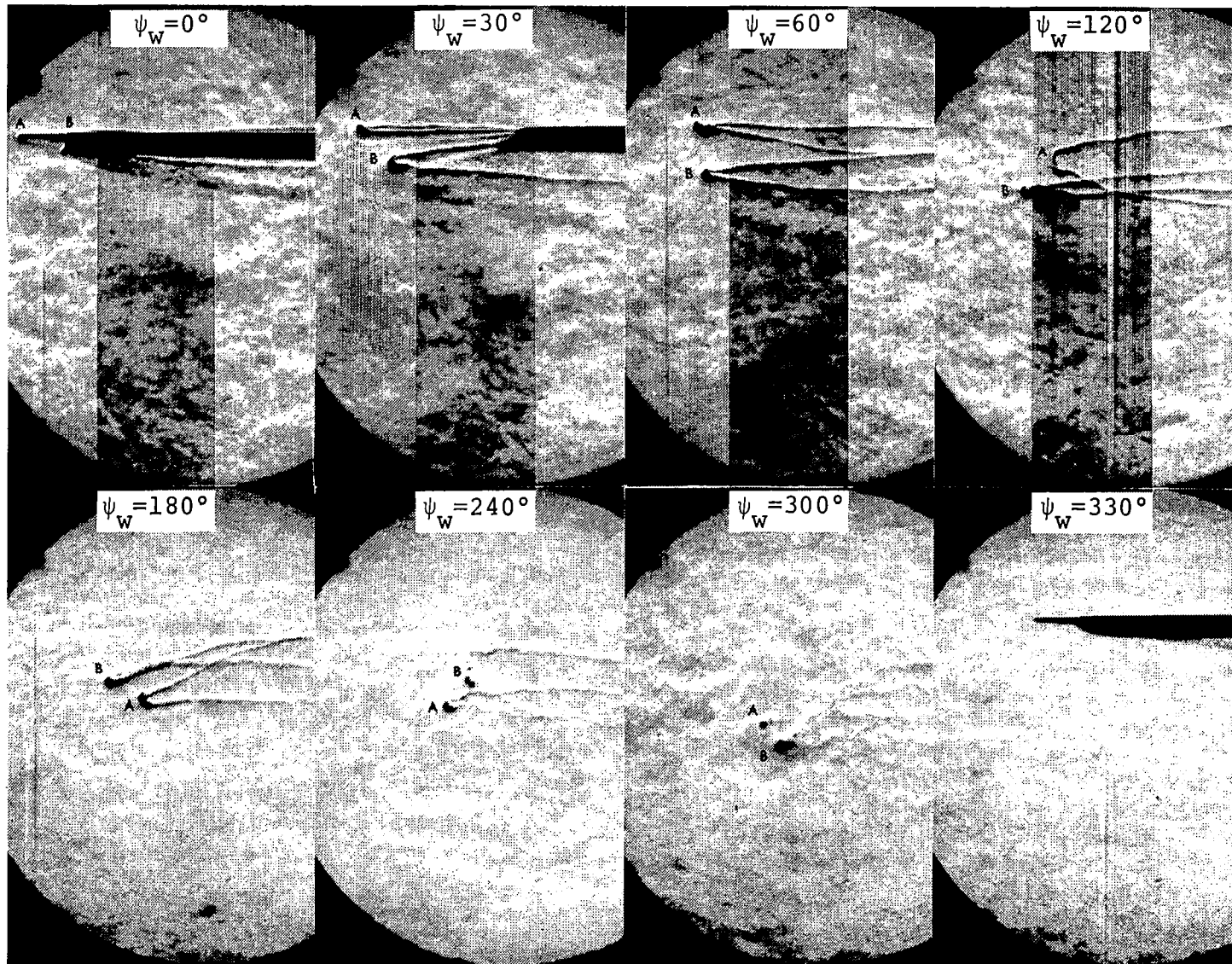
Figure 20.   Wake generated by the subwing tip (c=0.20C, NACA 0012 airfoil)
rotor at θ=9°, b=1, V_T=152 m/sec.

Figure 21.   Wake generated by the subwing tip (c=0.20C, NACA 0016 airfoil)
rotor at θ=6°, b=1, V_T=152 m/sec.

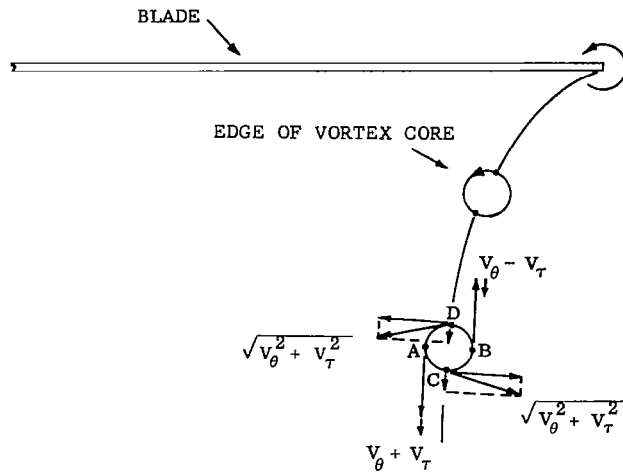Figure 22. Wake generated by the subwing tip (c=0.18C, NACA 0016 airfoil) rotor at $\theta=6°$, b=1, $V_T=152$ m/sec.

Figure 23. Wake generated by the subwing tip (c=0.18C, NACA 0016 airfoil) rotor at $\theta=9°$, b=1, $V_T=152$ m/sec.

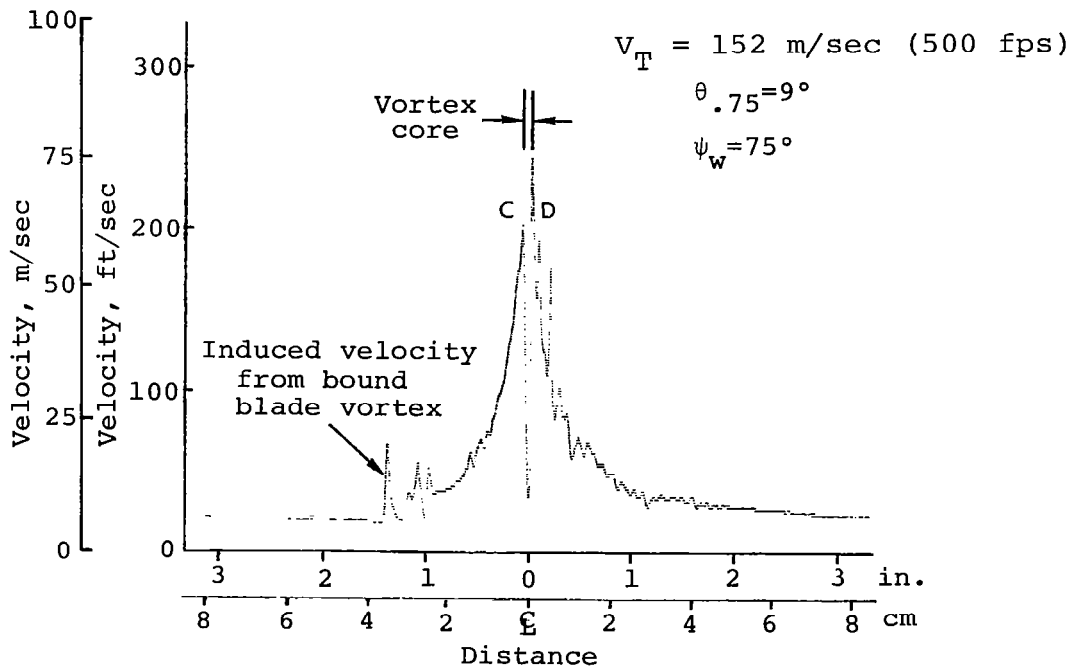Figure 24. Analysis of the vortex core intersecting the hot-wire.

Figure 25. Hot-wire anemometer measurement of the velocity distribution through the tip vortex of the square tip.
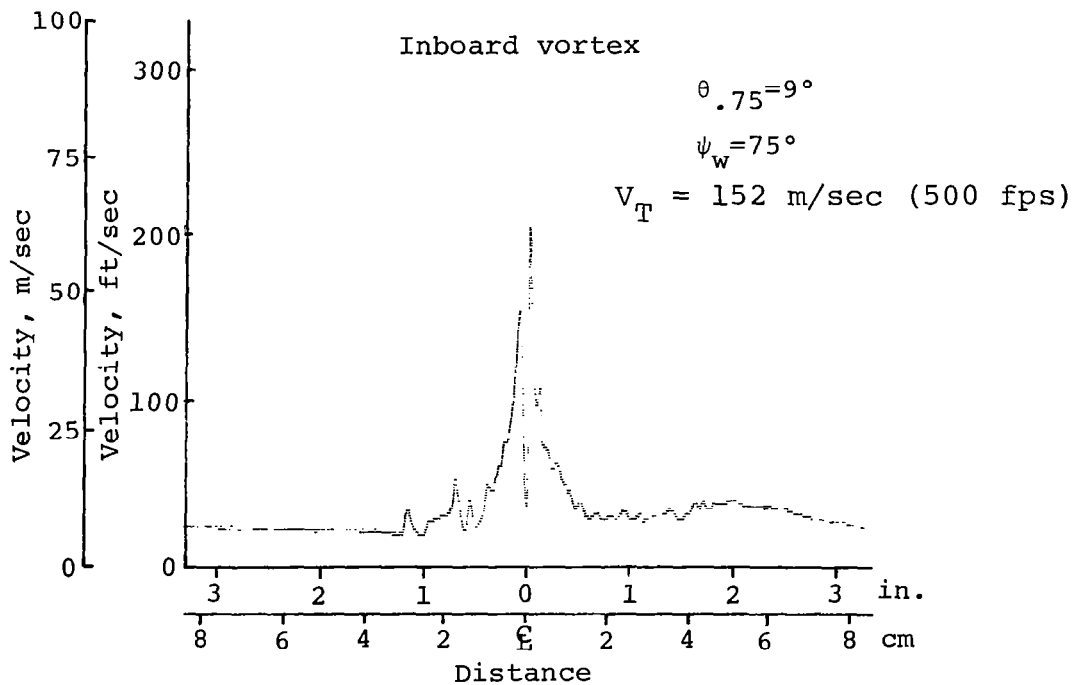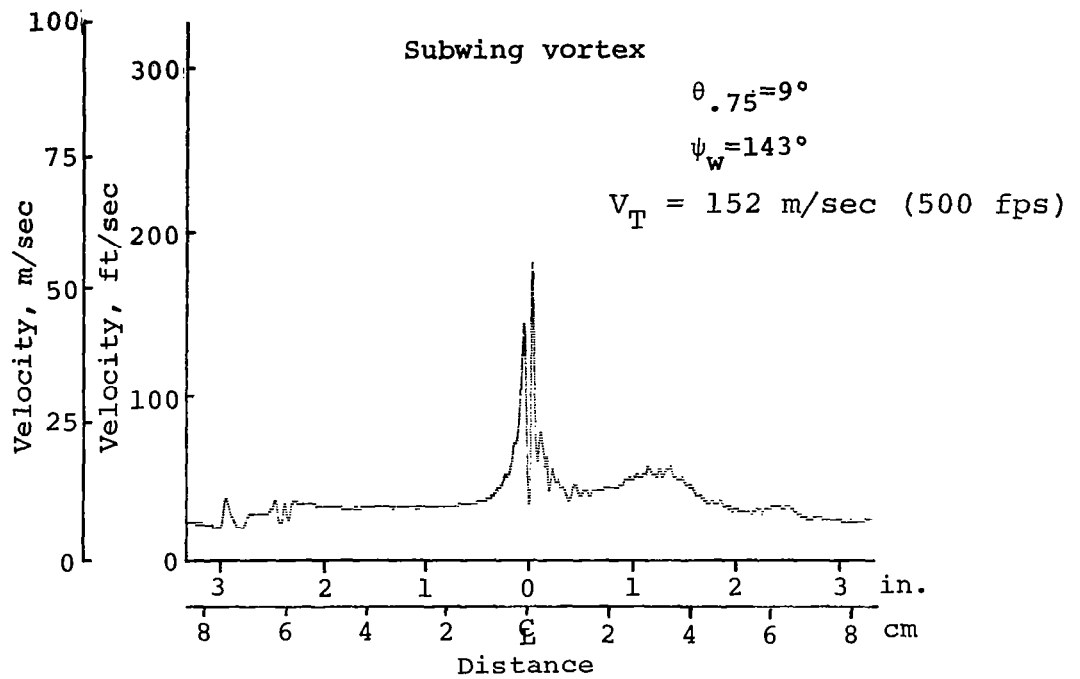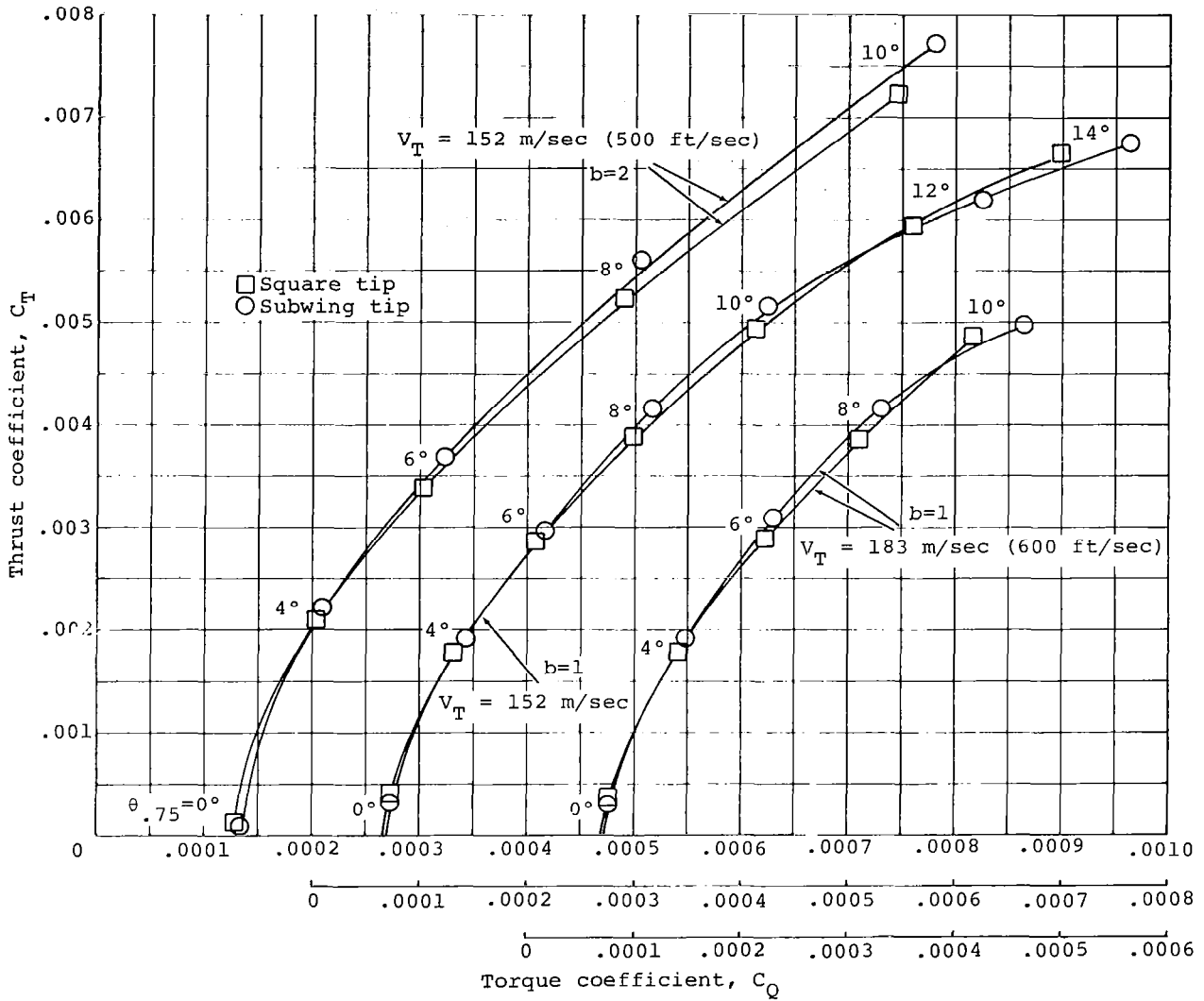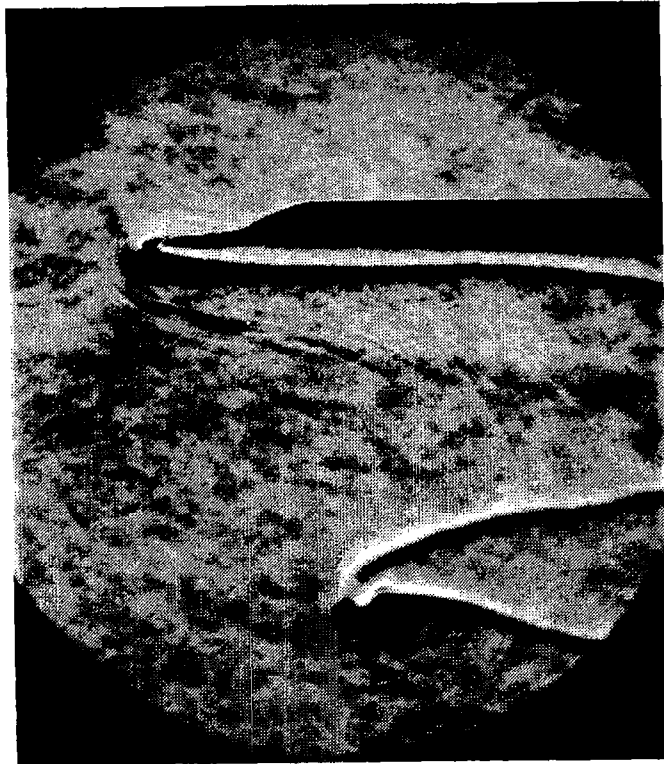
Figure 26. Hot-wire anemometer measurement of the velocity distribution through the tip vortices for the subwing tip (c=0.20C, NACA 0012 airfoil).
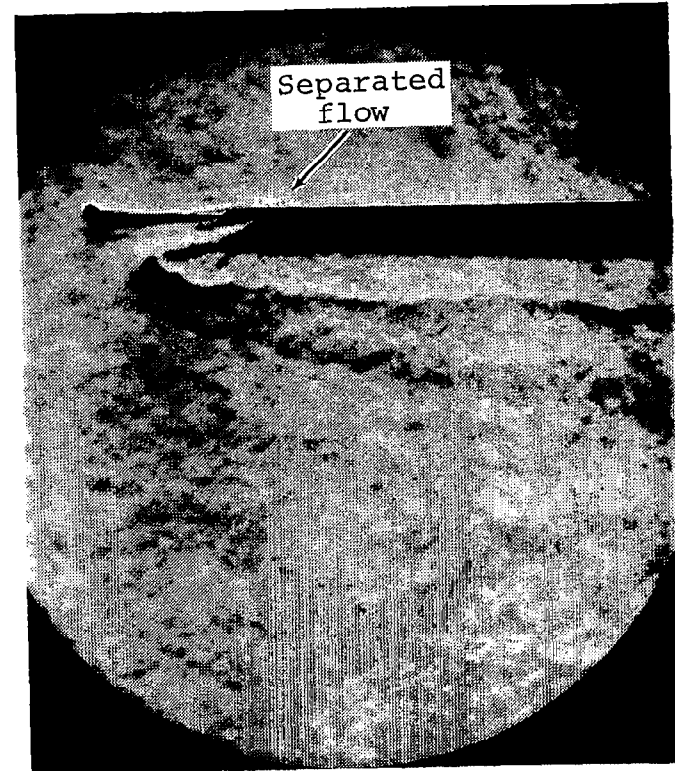
42

Figure 27. Performance comparison between the square tip and subwing in a one and two-bladed configuration.

$\rho = 1.15$ kg/m³ (0.00225 slugs/ft³)
$R = 61$ cm (24 in.)

Square tip   Subwing tip

Figure 28.   Comparison of the wake structure generated by the
             square tip and subwing for θ=12°.

1. Report No. NASA CR-3058	2. Government Accession No.	3. Recipient's Catalog No.
4. Title and Subtitle Experimental Investigation of the Subwing Tip and Its Vortex Structure		5. Report Date November 1978
		6. Performing Organization Code
7. Author(s) James L. Tangler		8. Performing Organization Report No.
		10. Work Unit No.
9. Performing Organization Name and Address Bell Helicopter Textron Division of Textron Inc. Post Office Box 482 Fort Worth, TX 76101		
		11. Contract or Grant No. NAS1-14465
12. Sponsoring Agency Name and Address National Aeronautics & Space Administration Washington, DC 20546		13. Type of Report and Period Covered Contractor Report
		14. Sponsoring Agency Code

15. Supplementary Notes

16. Abstract

Vortex diffusion resulting from the interaction of twin vortices generated by a "subwing" tip was experimentally investigated. The purpose of the investigation was to provide a better understanding of the subwing's vortex structure relative to a square tip for several angle of attack and yaw angles. This comparison included subwings of various chord size and airfoil thickness. Flow visualization, together with performance and wake measurements, provided a comparison between the square tip and subwing tips during both a semi-span wind-tunnel test and a small-scale rotor hover-stand test.

Through these studies, the subwing chord to main chord ratio which generated twin vortices was found to be 0.20. When the tip shed circulation was divided into twin vortices, the maximum circumferential velocity in each vortex was lowered relative to a comparable square tip. The influence of yawed flow on the operation of the subwing was not a significant factor for yaw angles corresponding to those that occur on a helicopter rotor blade during partial power descent. Comparisons of subwings having different airfoil thicknesses showed this parameter to be unimportant. No noticeable difference in performance between the subwing and square tip could be detected at medium rotor thrust coefficients.

17. Key Words (Suggested by Author(s)) Vortex Subwing Tip	18. Distribution Statement Unclassified - Unlimited Subject Category 02
19. Security Classif. (of this report) Unclassified	20. Security Classif. (of this page) Unclassified	21. No. of Pages 48	22. Price* $4.50